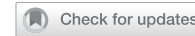


## ARTICLE

## OPEN



# Post-irradiation dietary restriction impairs hematopoiesis via inhibition of the pentose phosphate pathway in hematopoietic stem and progenitor cells

Si Tao<sup>1,7</sup>, Mingyue Su<sup>1,7</sup>, Chenghui Yu<sup>1</sup>, Xingxing Qiu<sup>1</sup>, Bing Zou<sup>1</sup>, Rongrong Qiu<sup>1</sup>, Yuanyuan Wu<sup>1</sup>, Lulu Liu<sup>2</sup>, Zhendong Tao<sup>3</sup>, Liu Zhang<sup>4</sup>, Hua Wang<sup>1</sup> and Duozhuang Tang<sup>1,5,6</sup>

© The Author(s) 2025

Although the clinical observation of hematologic toxicity related to radiotherapy has been recognized for a long time, the underlying mechanisms remain to be fully explored. Here, we established a mouse model of reduced dietary intake (dietary restriction, DR, 30% reduction in food intake compared to age-matched and gender-matched mice) following X-ray radiation exposure to investigate the impact of reduced dietary intake on hematopoiesis after irradiation. We found that post-irradiation DR significantly and persistently suppressed hematopoiesis and notably impaired the regenerative capacity of hematopoietic cells. Compared to ad libitum (AL) fed mice, post-irradiation DR led to sustained upregulation of the DNA damage response (DDR) signaling pathway in hematopoietic cells, even 14 days to 1 month after irradiation, along with delayed DNA repair. Further investigation revealed that DR suppressed the post-irradiation activation of the pentose phosphate pathway (PPP). Inhibition of PPP by 6-Aminonicotinamide (6-AN) in AL mice mimicked the impairment of hematopoiesis observed in DR mice, while activation of PPP by AG1 in DR mice rescued the impairment of DNA repair and hematopoiesis in these mice. Additionally, we conducted a retrospective analysis of 101 cancer patients who received pelvic radiotherapy and found that patients with lower Body Mass Index (BMI) experienced more severe reductions in white blood cells (WBCs), neutrophils, and lymphocytes. This study suggests that DR following irradiation inhibits hematopoiesis by suppressing PPP, providing a new approach to addressing radiotherapy-related myelosuppression and potentially offering solutions for improving refractory hematopoietic disorders associated with radiotherapy.

*Cell Death and Disease* (2026)17:8; <https://doi.org/10.1038/s41419-025-08249-w>

## INTRODUCTION

Radiation therapy is one of the main treatments for tumors, with radiation damage to non-tumor tissues being the most common side effect of radiotherapy [1]. The radiation fields of multiple malignant tumors (such as rectal cancer, anal cancer, prostate cancer, bladder cancer, and female reproductive tract tumors) involve hematopoietic tissues like flat bones and long bones. The hematopoietic system is extremely sensitive to radiation [2], with cytopenia being one of the most common complications of radiotherapy [3]. Complications such as recurrent severe leukopenia and increased susceptibility to infection related to radiotherapy, which can even be difficult to recover, may lead to treatment interruption, inability to tolerate subsequent treatments, and severely affect patient survival and prognosis [4].

Hematopoietic stem cell (HSC) function is influenced by multiple factors, including the condition of the HSCs themselves, local niches, and systemic environment [5]. Recent studies showed

that dietary restriction (30% reduction in food intake compared to age-matched and gender-matched mice) in non-irradiated (NIR) mice can induce a change in the differentiation tendency of HSCs and significantly inhibit lymphoid hematopoiesis, and continuous DR (dietary restriction) has a strong inhibitory effect on hematopoiesis under steady-state conditions [6, 7]. These studies suggest that reduced dietary intake has an important regulatory role on hematopoiesis under steady-state conditions, but its regulatory effect on irradiated HSCs and hematopoiesis remains to be elucidated. Caloric restriction (CR) has been shown to extend lifespan and slow aging, with its effects varying based on timing, degree, and individual factors [8, 9]. Early-life CR in rodents yields significant lifespan benefits, while adult-onset CR offers more modest effects [9]. Though CR reduces risks of chronic diseases and improves metabolic health, excessive restriction can cause adverse outcomes like anemia and muscle atrophy, especially in lean or elderly individuals [10]. Numerous studies have

<sup>1</sup>Department of Oncology, The Second Affiliated Hospital, Jiangxi Medical College, Nanchang University, Nanchang, Jiangxi, China. <sup>2</sup>Department of Medical Oncology, First Affiliated Hospital, School of Medicine, Zhejiang University, Hangzhou, Zhejiang, China. <sup>3</sup>Department of Medical Laboratory Medicine, Jiangxi Province Hospital of Integrated Chinese & Western Medicine, Nanchang, Jiangxi, China. <sup>4</sup>Intensive Care Unit, Beijing Jishuitan Hospital, Capital Medical University, Beijing, China. <sup>5</sup>Jiangxi Province Key Laboratory of Precision Cell Therapy (2024SSY06241), The Second Affiliated Hospital, Jiangxi Medical College, Nanchang University, Nanchang, Jiangxi, China. <sup>6</sup>Department of Hematology, The Second Affiliated Hospital, Jiangxi Medical College, Nanchang University, Nanchang, Jiangxi, China. <sup>7</sup>These authors contributed equally: Si Tao, Mingyue Su.

email: [nedefy11234@ncu.edu.cn](mailto:nedefy11234@ncu.edu.cn)

Edited by Professor Alessandro Finazzi-Agrò

Received: 1 April 2025 Revised: 10 October 2025 Accepted: 3 November 2025

Published online: 07 January 2026

highlighted the impact of diet on radiation response [11]. Dietary interventions, such as CR [12] and fatty acids [13], increase the radiosensitivity and oxidative DNA damage. Antioxidants (e.g., vitamins C and E, selenium, and polyphenols) have shown potential in mitigating oxidative stress, reducing inflammation, and protecting tissues [11]. Probiotics further contribute by supporting gut health and preventing radiation-induced gastrointestinal injury [14–16]. These findings underscore the critical role of diet in enhancing radiation tolerance and recovery.

Existing literature indicates that exposure to ionizing radiation can also induce significant damage to the bone marrow (BM) environment, which plays a crucial role in maintaining HSCs [17]. Yet whether post-irradiation DR would also have effects on the BM environment remains to be explored [18, 19].

HSCs are the source of hematopoiesis [20, 21]. Previous studies have reported that radiation can activate DNA damage signaling pathways in HSCs, leading to their hematopoietic dysfunction [22–24]. Radiation exposure also activates DNA repair pathways, which require DNA synthesis to varying extents. The pentose phosphate pathway (PPP) is a crucial metabolic route for glucose oxidation, providing ribose-5-phosphate (R5P) for RNA and DNA de novo synthesis, and Nicotinamide adenine dinucleotide phosphate (NADPH) for reductive biosynthesis (e.g., lipid and deoxyribose synthesis) and antioxidant defense. Studies in frog eggs [25] and cell lines [25, 26] have shown that the activation of glucose-6-phosphate dehydrogenase (G6PD, the rate-limiting enzyme of the oxidative branch of the PPP) is associated with increased PPP activity and is necessary for effective DNA repair [25, 27, 28]. However, the role of the PPP in the repair of hematopoietic cell damage following radiation exposure has not been studied.

Overall, HSC regulation after radiation injury involves multiple mechanisms: radiation damages HSCs directly, and also impairs the BM environment, which supports HSC regeneration [5, 22]. Despite these known mechanisms, the role of DR and the PPP in regulating hematopoiesis post-radiation remains unclear.

Tumor patients often experience reduced appetite and decreased dietary intake due to disease, treatment, and psychological factors, leading to weight loss and a decrease in body mass index (BMI) [29]. It is common for patients undergoing radiotherapy to simultaneously receive chemotherapy, which can further exacerbate appetite reduction and decreased dietary intake. Many studies have shown that clinically, patients receiving radiotherapy commonly experience reduced dietary intake [30]. Some studies suggest that obesity may increase the incidence and overall mortality in patients with major diseases such as cancer [31] or heart failure [32], while other studies indicate that obesity can have a protective effect on patient survival in certain cases [33–35]. These findings have sparked discussions about the obesity paradox, suggesting that obesity may offer protective benefits under specific conditions. It remains unclear whether dietary intake and nutritional status play a role in the regulation of hematopoiesis after radiation damage.

To investigate the impact of reduced dietary intake on hematopoiesis after irradiation, we first established a mouse model of reduced dietary intake (dietary restriction, DR) in C57BL/6 J mice following X-ray radiation exposure. We found that post-irradiation DR significantly and persistently suppressed hematopoiesis and notably impaired the regeneration capacity of HSCs. Comparing to ad libitum (AL) fed mice, post-irradiation DR in these mice led to sustained upregulation of the DNA damage response (DDR) signaling pathway in hematopoietic cells, even 14 days to 1 month after irradiation, along with delayed DNA repair. Further investigation revealed that DR inhibits DNA repair and reduces the anti-reactive oxygen species (ROS) response by suppressing the post-irradiation activation of the PPP, thereby inhibiting hematopoiesis. We also conducted a retrospective analysis of the relationship between blood routine

test results and BMI in 101 cancer patients who received pelvic radiotherapy. We found that patients with lower BMI had more severe reductions in white blood cells (WBCs), neutrophils, and lymphocytes. Therefore, we hypothesize that post-irradiation food restriction suppresses PPP in HSCs, thereby reducing the supply of precursors for DNA synthesis and inhibiting DNA repair. This study suggests that DR following irradiation inhibits hematopoiesis by suppressing the PPP, providing a new approach to addressing radiotherapy-related myelosuppression and potentially offering solutions for improving refractory hematopoietic disorders associated with radiotherapy.

## METHODS AND MATERIAL

### Mice and dietary intervention

Female C57BL/6J mice aged 2 months were maintained on a 12-h light/dark cycle under specific pathogen-free conditions. Mice were housed individually so that the daily food consumption of each mouse could be determined. This was measured every day for one week to determine their AL-feeding rate. After the 1-week measurement, the average amount of food was determined for every mouse. Animals were randomized into different groups ( $n = 5$  mice per group from 1 experiment representative of 2 independent experiments). During the feeding protocol, the ad libitum (AL) mice were fed with unlimited access to food, while DR mice were fed with 70% the average amount of food according to the previous calculation. The calculated 70% food pellet was added to each cage daily at the same time, and was constant over the whole DR period. The mice were fed a commercially formulated diet specifically designed for the growth and reproduction of rats and mice (Tianjin Ke'shi Feed Co., Ltd., Product No. 101670654803973120). The diet ingredients included corn, soybean meal, fish meal, wheat flour, yeast powder, vegetable oil, salt, and various vitamins and mineral elements. The guaranteed nutritional composition was as follows: moisture  $\leq 10\%$ , crude fat  $\geq 4\%$ , crude ash  $\leq 8\%$ , crude protein  $\geq 20\%$ , crude fiber  $\leq 5\%$ , calcium 1.0–1.8%, and phosphorus 0.6–1.2%. Detailed nutritional analysis values (per kilogram content) are provided in Supplementary Table 1. Animal experiment has been reviewed and approved by the Animal Ethics Committee of Nanchang Leyou Biotechnology Co., Ltd., with the approval number RYE2022062801. Sample size was chosen empirically based on our previous experience in the calculation of experimental variability. The investigators were not blinded to allocation during the experiments and the evaluation of the results.

### Mouse irradiation

A commercial medical electronic linear accelerator (Elekta VersaHD) was used for the radiation experiments. The position of irradiated samples was set at source-to-surface distance 50 cm from the source of the machine. Around  $35 \times 35 \text{ cm}^2$  was set for the radiation field size. The beam used was 6 MV X-ray with a dose rate of 600 MU/min. The daily dose output was checked using a commercial Farmer ion chamber PTW 30013, which was calibrated by a secondary standard dosimetry laboratory. The prescribed doses used in this research were 4.5 and 9 Gy, respectively.

### Flow cytometry

Mouse BM cells were obtained by crushing all hind limbs in sterile Phosphate Buffered Saline (PBS) supplemented with 2% heat-inactivated fetal bovine serum and filtering through a 40  $\mu\text{m}$  cell strainer. BM cells were then resuspended in red blood cell (RBC) lysis buffer to remove RBCs, washed with sterile PBS, manually counted using a hemocytometer, and incubated with antibody mixtures for flow cytometric analysis to detect cell surface markers. For CMPs/GMPs/HSCs, the following antibodies were used: biotinylated anti-B220 (BioLegend, Clone: RA3-6B2, Cat. #103204), CD11b (BioLegend, Clone: M1/70, Cat. #101204),

Gr-1 (BioLegend, Clone: RB6-8C5, Cat. #108404), TER-119 (BioLegend, Clone: TER-119, Cat. #116204), CD4 (BioLegend, Clone: RM4-5, Cat. #100508), CD8 (BioLegend, Clone: 53-6.7, Cat. #100704), PE-Cy7-CD16/32 (BioLegend, Clone: 93, Cat. #101318), FITC-CD34 (BD, Clone: RAM34, Cat. #553733), APC-c-Kit (BioLegend, Clone: 2B8, Cat. #105812), PE-Sca-1 (BioLegend, Clone: D7, Cat. #108108), APC-Cy7-Streptavidin (BioLegend, Cat. #405208), PerCP/Cy5.5-CD150 (BioLegend, Clone: TC15-12F12.2, Cat. #115922). HSCs were defined as Lineage<sup>-</sup>; c-Kit<sup>+</sup>; Sca-1<sup>+</sup>; CD34<sup>-</sup> and CD150<sup>+</sup>. CMPs were defined as Lineage<sup>-</sup>; c-Kit<sup>+</sup>; Sca-1<sup>-</sup>; CD34<sup>+</sup> and CD16/32<sup>-</sup>. GMPs were defined as Lineage<sup>-</sup>; c-Kit<sup>+</sup>; Sca-1<sup>-</sup>; CD34<sup>+</sup> and CD16/32<sup>+</sup>. MEPs were defined as lineage<sup>-</sup>; c-Kit<sup>+</sup>; Sca-1<sup>-</sup>; CD34<sup>-</sup>; and CD16/32<sup>-</sup> cells. B220 cells in BM, peripheral blood, and spleen were stained with the APC-Cy7-B220 (BioLegend, Clone: RA3-6B2, Cat. #103224) antibody. Bone marrow resident macrophages (BMRMs) were stained with the FITC-CD169 (BioLegend, Clone: 3D6.112, Cat. #142406), PerCP/Cy5.5-CD115 (BioLegend, Clone: AFS98, Cat. #135526), PE-F4/80 (BioLegend, Clone: BM8, Cat. #123110), APC-Gr-1 (BioLegend, Clone: RB6-8C5, Cat. #108412) antibodies. BMRMs were defined as: Gr-1<sup>med/-</sup>, CD115<sup>-</sup>, F4/80<sup>+</sup>, SSC<sup>-</sup>, CD169<sup>+</sup>. For apoptosis analysis, the staining method for HSC surface markers included a mixture of biotinylated anti-B220 (Clone: RA3-6B2, Cat. #103204), CD11b (Clone: M1/70, Cat. #101204), Gr-1 (Clone: RB6-8C5, Cat. #108404), TER-119 (Clone: TER-119, Cat. #116204), CD4 (Clone: GK1.5, Cat. #100404), and CD8 (Clone: 53-6.7, Cat. #100704) antibodies (BioLegend), along with FITC-CD34 (BD, Clone: RAM34, Cat. #553733), APC-c-Kit (BioLegend, Clone: 2B8, Cat. #105812), PE-Cy7-Sca-1 (BioLegend, Clone: D7, Cat. #558162), APC-Cy7-Streptavidin (BioLegend, Cat. #405208), and PerCP/Cy5.5-CD150 (BioLegend, Clone: TC15-12F12.2, Cat. #115922). After staining, cells were fixed using paraformaldehyde (Servicebio, Cat. #G1101-500ml) and subsequently stained according to the manufacturer's instructions with the BD Pharmingen™ PE Annexin V Apoptosis Detection Kit I (BD, Cat. #559763). Cells were incubated in PE-Annexin V (Cat. #51-65875X) at room temperature in the dark for 15 min, followed by DAPI (Abcam, Cat. #abs42016321) binding buffer staining to detect DNA content. Stained cells were analyzed on a flow cytometer (FACs) (FACs Canto II; BD).

For ROS staining, CellROX™ Green (Thermo Fisher Scientific, cat. #C10492) was used to treat  $1 \times 10^6$  total BM cells to measure intracellular ROS levels. CellROX™ Green is a fluorescent probe that emits bright green, photostable fluorescence upon oxidation. For the negative control, 500  $\mu$ M N-acetylcysteine was added and incubated at 37 °C and 5% CO<sub>2</sub> for 1 h. Then, 200  $\mu$ M tert-butyl hydroperoxide was added to both the positive and negative controls and incubated under the same conditions for 30 min. Next, 250  $\mu$ M CellROX™ Green reagent was added to 1 ml of the cell suspension and incubated at room temperature, protected from light, for 30 min. Finally, the green fluorophore was excited by a 488 nm laser, and FACS (FACs Canto II; BD) was used for analysis. The gating was adjusted using the positive and negative controls, MIF = 1 in NIR AL mice.

### Sorting

For hematopoietic stem and progenitor cells (HSPCs) sorting, BM cells were labeled with APC anti-mouse CD117 (c-Kit) antibody (BioLegend, Clone: 2B8, Cat. #105812), incubated at 4 °C for 30 min in the dark, and then enriched and sorted using anti-APC MicroBeads (Miltenyi Biotec, Cat. #130-090-855) and LS Columns (Miltenyi Biotec, Catalog no. 130-122-729) following the manufacturer's instructions.

### 6-aminonicotinamide treatment

The 6-aminonicotinamide (6-AN) was purchased from MedChem-Express Co., Ltd, China (CAS No. 329-89-5; Lot number: HY-W010342; purity: 99.95%), and was diluted in saline for injection

intraperitoneally for 7 days post-irradiation. The daily dose of 6-AN was 10 mg/kg for young mice. In the control group, saline was injected instead of 6-AN.

### G6PD activator AG1 treatment

The G6PD activator AG1 was purchased from MedChemExpress Co., Ltd., China (CAS No. 421581-52-4; Lot number: HY-123962; purity: 99.54%), and was diluted in dimethyl sulfoxide (DMSO) for injection intraperitoneally every other day for 9 times post-irradiation. The daily dose of AG1 was 20 mg/kg for young mice. The control group was injected with an equal volume of DMSO.

### Sucrose water use

Sucrose was purchased from Servicebio Co., Ltd, China (CAS No. 57-50-1; Lot number: GC205014-500g; purity: analytical reagent). The sucrose drinking solution was prepared at a concentration of 50 g/L according to published protocols, with the solution being replaced every 2–3 days.

### G6PD activity determination

G6PDH activity was measured using a commercial kit (#S0189, Beyotime, Shanghai, China) according to the manufacturer's instructions. Briefly,  $1 \times 10^6$  total BM cells were treated with 200  $\mu$ L extraction buffer, centrifuged at 12,000  $\times g$  for 10 min, and 50  $\mu$ L of supernatant was incubated with 50  $\mu$ L of G6PDH working solution in the dark at room temperature for 10 min. Absorbance was measured at 450 nm.

### NADPH content determination

NADPH content was assessed using a NADPH detection kit (#S0179, Beyotime, Shanghai, China) according to the manufacturer's instructions. Briefly,  $1 \times 10^6$  total BM cells were treated with 200  $\mu$ L extraction buffer, centrifuged at 10,000  $\times g$  for 10 min, and the supernatant was incubated at 60 °C for 30 min to decompose NADP. After cooling on ice, the supernatant was reacted with the working solution at 37 °C for 20 min, and absorbance was measured at 450 nm.

### Transplantation

For the primary BM transplantation,  $2 \times 10^6$  BM cells from irradiated Ly5.2 donor mice were mixed with  $1 \times 10^6$  BM cells from Ly5.1/5.2 heterozygous competitor mice and injected into lethally irradiated (9 Gy) Ly5.1 recipient mice for competitive transplantation. Four months post-primary transplantation,  $10 \times 10^6$  BM cells from the primary recipients were serially transplanted into lethally irradiated (9 Gy) Ly5.1 recipient mice. Peripheral blood (PB) analyses of the primary and secondary transplants were performed at 1–4 months after transplantation. The Ly5.1/5.2 competitor mice correspond to NIR AL mice.

### Immunofluorescence staining

C-Kit<sup>+</sup> cells were resuspended to  $1 \times 10^2$  cells/ $\mu$ L, dropped onto positively charged slides (Thermo, Catalog no. 4951PLUS), fixed with 4% paraformaldehyde (Servicebio, Catalog no. G1101) at room temperature (RT) for 10 min, permeabilized with 0.25% Triton/PBS at RT for 10 min, and blocked with 1% Bovine Serum Albumin (BSA)/PBS at RT for 1 h. Cells were then incubated overnight at 4 °C with anti-phosphorylated histone H2AX antibody (Abcam, Catalog no. Ser139, Cat. #ab22551) and Anti-53BP1 antibodies (Abcam, Cat. #ab175933) at 1:200 dilution, followed by incubation with anti-mouse Alexa Fluor 488 secondary antibody (Abcam, Cat. #ab237174) and anti-rabbit Alexa Fluor 594 secondary antibody (Abcam, Cat. #ab150080) at 1:400 dilution at RT for 1 h. Nuclei were counterstained with DAPI. Images were acquired on a Leica SP5 fluorescence microscope and processed with LAS-AF-Lite\_2.6.0. Foci in 250 c-Kit<sup>+</sup> cells per group were manually counted and analyzed.

BM cells were washed with ice PBS twice, and then fixed with 4% paraformaldehyde (Servicebio, Cat. no. G1101) at room temperature (RT) for 10 min, permeabilized with 0.25% Triton/PBS at RT for 10 min, and blocked with 1% BSA/PBS at RT for 1 h. After blocking, cells were incubated with Nrf2 Polyclonal Antibody (1:200, Invitrogen, ThermoFisher, Cat. #PA5-27882) overnight at 4 °C. After washing, cells were incubated for 1 h with Alexa Fluor 488 (1:400, Invitrogen, ThermoFisher, Cat. #A31731) secondary antibody at 37 °C and stained with DAPI to label cell nuclei. The signals were visualized, and digital images were obtained by the fluorescence stereoscope (Olympus SZX16). Foci in 250 BM cells per group were manually counted and analyzed.

#### Comet assay

Sorted c-Kit<sup>+</sup> cells were resuspended in PBS at  $1 \times 10^6$  cells/ml, mixed with 0.5% low-melting-point agarose (Beyotime, Cat. no. 39346-81-1), and quickly spread onto slides pre-coated with 0.8% normal-melting-point agarose (Thermo, Cat. no. 16500100). Slides were solidified at 4 °C for about 5 min, lysed under alkaline conditions for 1–2 h, and electrophoresed at 4 °C with buffer pH > 13. After electrophoresis, DNA was stained with propidium iodide (MCE, Cat. no. HY-D0815). DNA damage was observed under a fluorescence microscope (Nikon), and tail DNA percentage was analyzed using CASP software.

#### HE staining

Femurs were collected and fixed in 4% paraformaldehyde (Servicebio, Catalog no. G1101) at RT for 24 h, decalcified in 0.5 M EDTA (pH = 7.4, Servicebio, China, G1105) for 2 weeks, and then embedded in paraffin. Sections were cut at a thickness of 5 µm. Paraffin sections were deparaffinized in xylene twice for 20 min, rehydrated in gradient alcohol, stained with hematoxylin (Servicebio, Catalog no. G1001) for 5 min, washed with tap water, counterstained with eosin (Servicebio, Catalog no. G1004) for 5 min, dehydrated in gradient alcohol, and cleared in xylene. Sections were mounted with neutral gum and examined under a light microscope (Nikon).

#### Oil red O staining

Oil red O staining was performed according to BioVision's manual (BioVision). Briefly, femur frozen sections were equilibrated to RT, washed with 60% isopropanol (MCE, Catalog no. 67-63-0), stained with oil red O solution (Sigma-Aldrich, Cat. no. O1391) at 37 °C for 15 min, counterstained with hematoxylin (Servicebio, Catalog no. G1001) for 10 min, mounted with glycerol gelatin, and examined under a light microscope (Nikon).

#### Total RNA extraction and reverse transcription

Total RNA from cell samples was extracted using RNeasy Simple Total RNA Kit (TianGen Biotech) and reverse-transcribed using RevertAid First Strand cDNA Synthesis Kit (Thermo Scientific) according to the manufacturer's instructions. The process included incubation at 42 °C for 60 min and inactivation at 70 °C for 5 min.

#### Real-time quantitative PCR (qPCR)

qRT-PCR was performed using TransStart Tip Green qPCR Super-Mix (TransGen Biotech) on an ABI 7900 real-time PCR system (Applied Biosystems) in triplicate. Reaction conditions were: 94 °C for 30 s, followed by 40 cycles of 94 °C for 30 s and 60 °C for 30 s. Relative gene expression was normalized to β-actin in each sample, with the NIR AL group normalized to 1. Primer sequences used were listed in Supplementary Table 2.

#### Peripheral blood cell counting

PB was collected from the orbital venous plexus into tubes containing 0.5 M EDTA. PB cell counts were assessed using an automated blood analyzer (Sysmex, XS-500i).

#### Clinical data collection

Clinical data were retrospectively collected from 101 patients receiving radiotherapy at the Second Affiliated Hospital of Nanchang University. Data collection began on the first day of radiotherapy, and the BMI values, as well as the absolute counts of WBCs, lymphocytes, monocytes, RBCs, and platelets, were recorded weekly for the patients over a period of one month. The groups with differences were used to plot the receiver operating characteristic curve (ROC) and calculate the area under the curve (AUC) value to evaluate the model quality and select the optimal model threshold. The use of human data in this study was approved by the Institutional Ethics Committee of the Second Affiliated Hospital of Nanchang University (Approval No. MR-36-25-024749). Informed consent was waived by the Institutional Ethics Committee of the Second Affiliated Hospital of Nanchang University because of the retrospective nature of this study. All procedures involving human data adhered to the Declaration of Helsinki (2013 revision). As this was a retrospective study, the requirement for informed consent was waived by the Institutional Ethics Committee. Baseline demographics and disease characteristics of patients ( $n = 101$ ) are presented in Supplementary Table 3.

#### Radiotherapy and pelvic bone marrow delineation

The radiotherapy was performed using either intensity modulated radiotherapy (IMRT) or volumetric modulated radiotherapy (VMAT) with an Elekta linear accelerator (Elekta Versa HD, Sweden). The pelvic BM and other organs at risk (OARs) were contoured by a commercial segmentation software that worked with an artificial intelligence algorithm. Contouring of the targets (GTV, CTV) was performed by the same senior physician, and the treatment plans were designed by the same experienced dosimetrist. The mean dose (Dmean) of pelvic BM was obtained from the dose-volume histogram (DVH) curves calculated by the treatment planning system Monaco (Elekta, Sweden).

#### Statistical analysis

All data were analyzed using GraphPad Prism 9.0 software. Two-group datasets were analyzed using Student's *t*-tests. For comparison among different groups, one-way or two-way ANOVA was used, with Tukey's multiple comparisons test was used to calculate *p*-values. Specific data analyses were described in each figure legend. The variance was similar between the groups that were being statistically compared. The results are presented as the mean  $\pm$  SD. All in vitro experiments were conducted in two independent experiments.  $p < 0.05$  was considered statistically significant. Statistical significance was denoted as  $^*p < 0.05$ ,  $^{**}p < 0.01$ ,  $^{***}p < 0.001$ ,  $^{****}p < 0.0001$  and "ns" indicates no significant difference. The number of animals used in each experiment is indicated in the corresponding figure legend. The samples in this study represent biological replicates. Each replicate was independently obtained from different mice under identical experimental conditions. Specifically, BM cells were collected from five mice per group, with each mouse considered as one biological replicate.

## RESULTS

#### Post-irradiation DR significantly inhibits hematopoiesis

To investigate the effects of post-irradiation DR on hematopoiesis, we used a mouse model where mice were subjected to 4.5 Gy irradiation followed by a DR diet (70% of the intake of age- and sex-matched AL fed mice) (Fig. 1A). We first examined the effects of DR on body weight in mice (Fig. 1B). Under both non-irradiation and irradiation conditions, the body weight ratio of mice comparing to the initial timepoint increased in AL group, while it decreased in the DR group over time (Fig. 1B). In the DR group, the median body weight ratio was 0.913 under NIR condition and

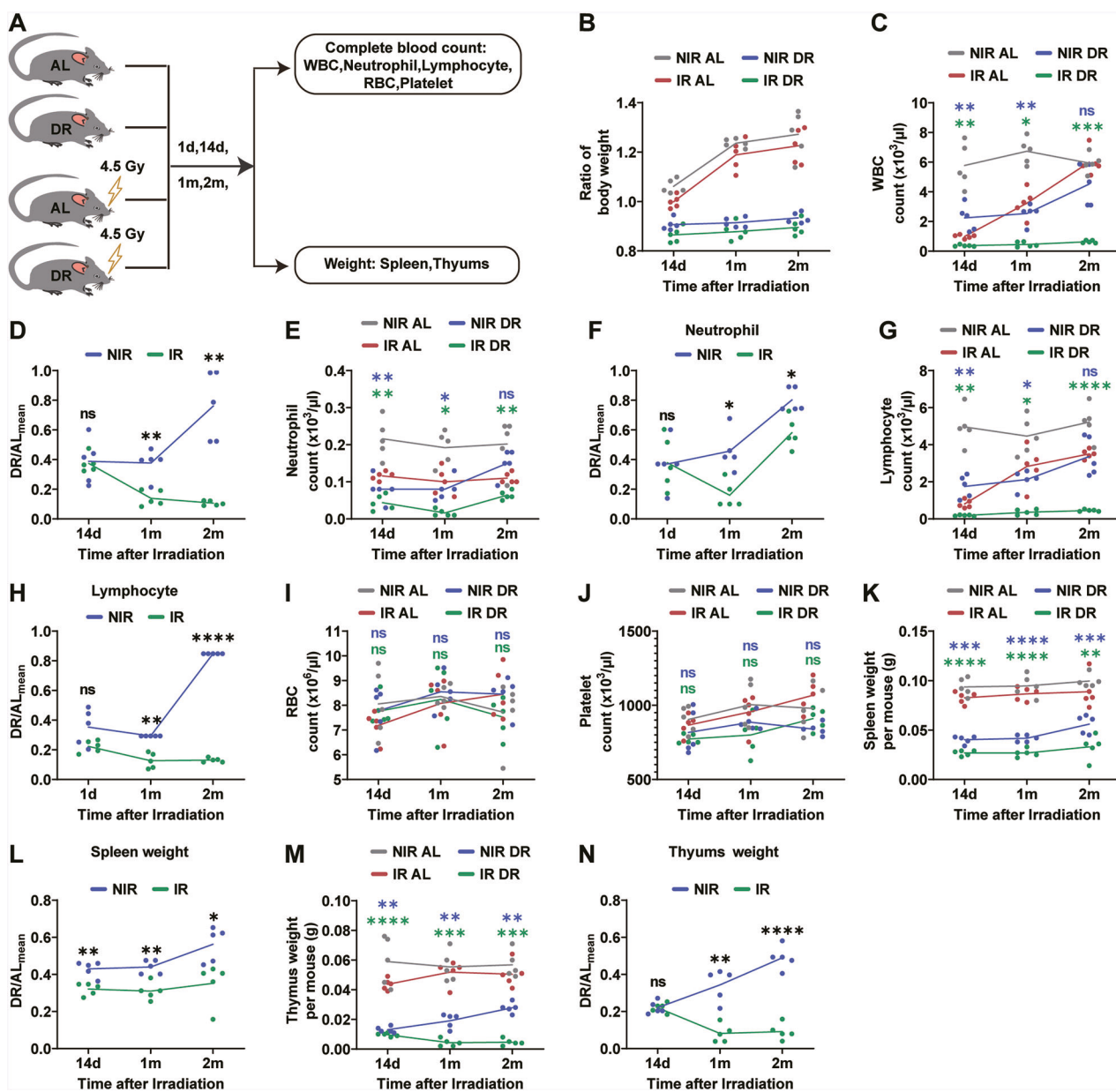
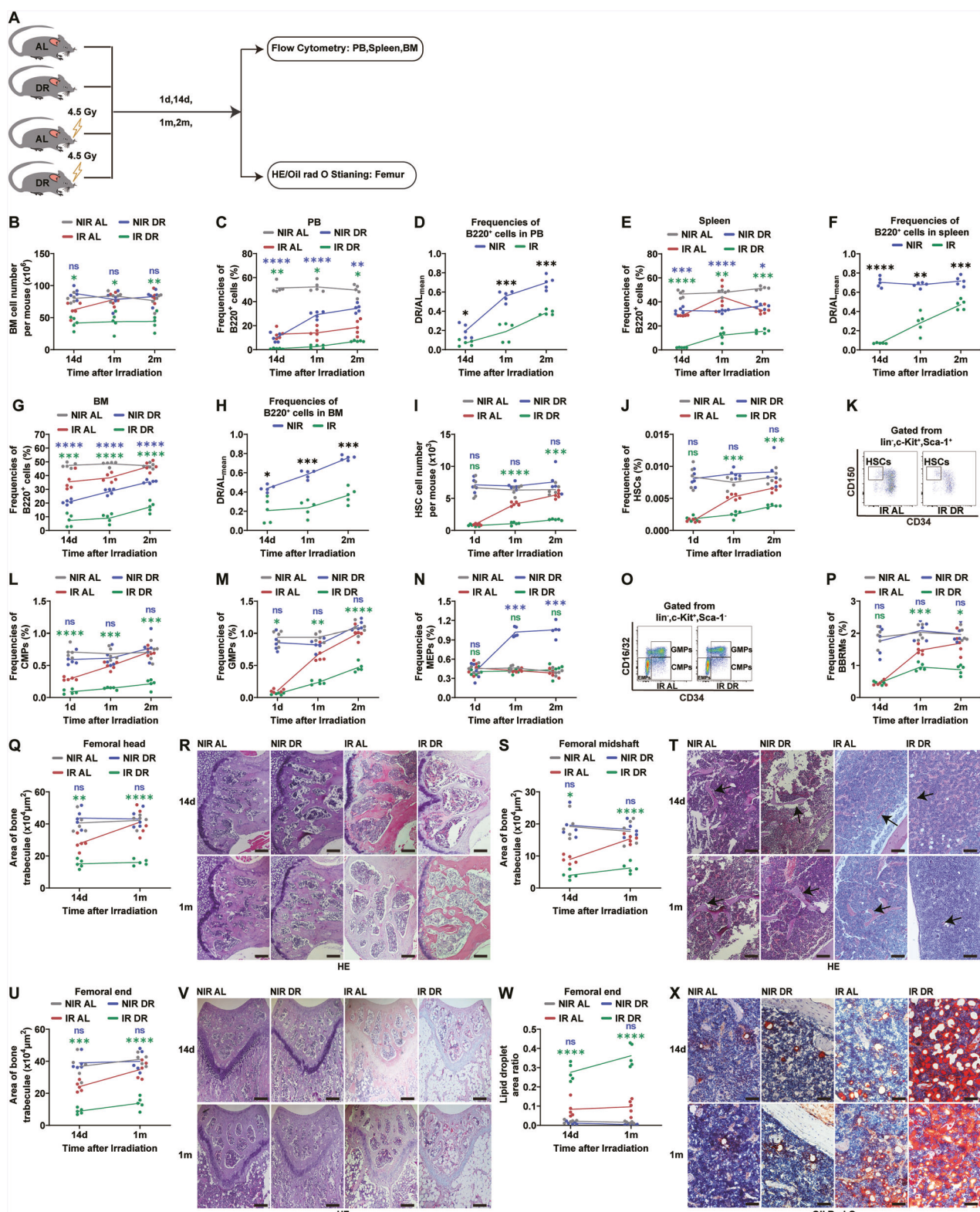


**Fig. 1 Suppression of body weight and peripheral blood in mice by DR post-irradiation.** **A** Experimental scheme. Wild-type C57BL/6 mice (2 months old) were irradiated with 4.5 Gy X-rays, fed with either AL diet or DR diet (daily food intake restricted to 70% of the intake of age- and sex-matched AL mice). NIR mice receiving an AL or DR diet were also monitored as a control ( $n = 5$  mice per group from 1 experiment representative of 2 independent experiments). **B** Ratio of body weight of mice at the indicated time points to the average initial body weight post-irradiation and no irradiation. **C–J** PB cell counting at the indicated time points. Absolute counting value of WBC (**C**), Neutrophil (**E**), Lymphocytes (**G**), RBC (**I**) and Platelet (**J**). **D, F, H** Ratio of the number of WBC (**D**), Neutrophil (**F**), Lymphocytes (**H**) in DR mice at each time point to the average number in AL mice. Spleen (**K**) and thymus weight (**M**) at the indicated time points. Ratio of spleen weight (**L**) and thymus weight (**N**) in DR mice at each time point to the average spleen or thymus weight in AL mice. Results were displayed as mean  $\pm$  SD; ns, not significant; \* $p < 0.05$ ; \*\* $p < 0.01$ ; \*\*\* $p < 0.001$ ; \*\*\*\* $p < 0.0001$  by Two-way ANOVA test and multiple comparisons. AL ad libitum feeding, DR dietary restriction, NIR AL no irradiated ad libitum group, NIR DR no irradiated dietary restriction group, IR AL irradiated ad libitum group, IR DR irradiated dietary restriction group, WBC white blood cell, RBC red blood cell, d days, m months. The purple symbols indicate statistical significance between the non-irradiated groups. The green symbols indicate statistical significance between the irradiated groups.

0.888 under irradiated condition, indicating a median decrease of 8.7% in the NIR DR mice and 11.2% in IR DR mice. Notably, the maximum weight loss observed was <20% in all the groups, and we observed no significant deterioration in the general health of the mice (Fig. 1B). Hematological parameters were analyzed by PB cell counting and flow cytometric analysis at various time points post-irradiation. Results indicated that, under irradiation conditions, DR mice showed significantly lower counts of total WBCs, neutrophils, and lymphocytes compared to AL mice from two

weeks up to two months post-irradiation (Fig. 1C–H). However, there were no significant effects on RBCs and platelet counts (Fig. 1I and J). The spleen and thymus weights were also significantly lower in DR mice compared to AL mice (Fig. 1K–N). We subsequently performed flow cytometric analysis of PB, spleen, and BM cells to determine their frequencies, and conducted Oil Red O and hematoxylin–eosin (H&E) staining on mouse femurs (Fig. 2A), and BM cell counts were significantly reduced (Fig. 2B). Flow cytometric analysis showed that the frequencies of B cells



(B220<sup>+</sup> cells) in peripheral blood, spleen, and BM were consistently lower in DR mice than in AL mice (Fig. 2C–H). Further studies on the frequencies of HSCs (CD150<sup>+</sup> CD34<sup>−</sup> c-Kit<sup>+</sup> Sca-1<sup>+</sup>lineage<sup>−</sup> cells) and progenitor cells revealed that the frequencies of HSCs and HSC numbers in DR mice were significantly lower than in AL mice from one month up to 10 months post-irradiation (Fig. 2I–K).

Similarly, the frequencies of CMPs (CD16/32<sup>-</sup>CD34<sup>+</sup>c-Kit<sup>+</sup>Sca-1<sup>-</sup>lineage<sup>-</sup> cells) and GMPs (CD16/32<sup>+</sup>CD34<sup>+</sup>c-Kit<sup>+</sup>Sca-1<sup>-</sup>lineage<sup>-</sup> cells) in the BM were persistently lower in DR mice (Fig. 2L, M, O). We analyzed MEPs (CD16/32<sup>-</sup>CD34<sup>-</sup>c-Kit<sup>+</sup>Sca-1<sup>-</sup>lineage<sup>-</sup> cells) and found that under non-irradiation conditions, DR increased MEP frequency compared with AL feeding. However, following IR,

**Fig. 2 Suppression of hematopoiesis and damage to hematopoietic microenvironment in mice by DR post-irradiation.** **A** Experimental scheme. Wild-type C57BL/6 mice (2 months old) were irradiated with 4.5 Gy X-rays, fed with either AL diet or DR diet (daily food intake restricted to 70% of the intake of age- and sex-matched AL mice). NIR mice receiving AL or DR diet were also monitored as a control ( $n = 5$  mice per group from 1 experiment representative of 2 independent experiments). **B** Total BM cells counts at indicated time points post-irradiation and no irradiation. FACS analysis of frequencies of B220<sup>+</sup> lymphocytes in PB (**C**, **D**), spleen (**E**, **F**), BM (**G**, **H**); and frequencies of HSCs (**J**), CMPs (**L**), GMPs (**M**), MEPs (**N**) and BMRMs (**P**), and absolute number of HSCs (**I**) in BM. **C**, **E**, **F** Absolute value of frequencies. Ratio of frequencies of PB B220<sup>+</sup> cells (**D**), spleen B220<sup>+</sup> cells (**F**), and BM B220<sup>+</sup> cells (**H**) in DR mice at each time point to the average frequencies in AL mice. Representative FACS Plots of HSCs (**K**) and CMPs/GMPs/MEPs (**O**). Bone trabecular area in the femoral head, the femoral midshaft and the femoral end. **Q**, **S**, **U** Quantitative analysis of areas and **R**, **T**, **V** representative H&E staining images (scale bar: 100  $\mu$ m) at indicated time points post-irradiation and no irradiation. **W** and **X** Quantitative analysis of fat droplet area ratio in the femoral end and representative oil red O staining images (scale bar: 100  $\mu$ m) at indicated time points post-irradiation and no irradiation. Results were displayed as mean  $\pm$  SD; ns, not significant; \* $p < 0.05$ ; \*\* $p < 0.01$ ; \*\*\* $p < 0.001$ ; \*\*\*\* $p < 0.0001$  by Two-way ANOVA test with Tukey's multiple comparisons test. BM bone marrow, PB peripheral blood, HSC hematopoietic stem cell, CMPs common myeloid progenitors, GMPs granulocyte-macrophage progenitors, MEPs megakaryocyte-erythrocyte progenitors, BMRMs bone marrow resident macrophages. The purple symbols indicate statistical significance between the non-irradiated groups. The green symbols indicate statistical significance between the irradiated groups.

MEP frequency did not differ significantly between DR and AL groups (Fig. 2N, O). In our previous studies, we primarily focused on the effects of DR on the hematopoietic system under non-irradiation conditions. In this study, we again used NIR mice as controls and compared the effects of DR on hematopoiesis under irradiation conditions versus non-irradiation conditions. In consistency with our previous findings, DR led to a decrease in peripheral WBCs, neutrophils, and lymphocyte counts under non-irradiation conditions (Fig. 1C–H), and FACS also revealed a reduction in peripheral lymphocyte counts (Fig. 2C, D). Additionally, a decrease in the weight of lymphoid organs, such as the spleen and thymus (Fig. 1K–N), was observed. However, compared to the NIR group, the DR-induced reduction in peripheral WBCs, neutrophils, and lymphocytes was more pronounced in the irradiated group (Fig. 1C–H). Notably, at the two-month post-irradiation time point, the difference in peripheral WBCs between DR and AL groups was no longer significant in the NIR group (Fig. 1C, D). In contrast, in the irradiated group, the DR group still exhibited significantly lower levels of peripheral white blood cells compared to the AL group (Fig. 1C, D). Similarly, nitrification and lymphocyte counts (Fig. 1E–H), as well as the proportion of lymphocytes in the PB, spleen, and BM (Fig. 2C–H), remained significantly lower in the DR group compared to the AL group in the irradiated group at the two-month time point, with a greater magnitude of reduction than that observed in the NIR groups (Figs. 1E–H, 2C–F). These results suggest that DR significantly inhibits hematopoiesis post-irradiation, with this inhibitory effect being sustained over a relatively extended period and affecting various hematopoietic levels from HSCs to downstream peripheral lymphoid organs and PB cell counts.

#### Post-irradiation DR disturbs recovery of bone marrow environment

We further investigated the effects of DR on the BM environment. BMRMs which are located within the mesenchymal niche, play a crucial role in retaining HSCs within their niche, maintaining their quiescence, and protecting them from oxidative stress [36]. We examined frequencies of BMRMs by FACS analysis. In NIR mice, there was no significant difference in BMRMs between the AL and DR groups (Fig. 2P). However, at day 14 post-irradiation, a significant reduction in BMRMs was observed in both AL and DR mice (Fig. 2P). During the post-irradiation period, BMRMs in the AL group gradually recovered, returning to pre-irradiation levels by 2 months post-irradiation (Fig. 2P). In contrast, the DR group exhibited a sustained reduction in BMRMs (Fig. 2P). These findings suggest that post-irradiation DR can significantly suppress the recovery of BMRMs.

Previous studies have shown that irradiation leads to significant reductions in bone trabeculae area and increases in fat droplets in BM [37], which are closely related to reduced HSC and hematopoietic cell numbers and function. Osteoblasts in the

femur are known to promote hematopoiesis, and one result of osteoblast activity is increased bone trabeculae [17]. To investigate the impact of DR on the BM environment, we performed BM sections of femurs from DR and AL mice under non-irradiation conditions as well as irradiation conditions, and compared bone trabeculae in the femoral head, femoral midshaft, and femoral end (Fig. 2Q–V). DR showed a neutral effect on bone trabeculae and fat droplets in NIR mice (Fig. 2W, X). Notably, we found that bone trabeculae in IR AL mice were relatively continuous and intact, while those in IR DR mice were thinner and discontinuous. Quantitative analysis revealed that the bone trabeculae area in IR DR mice was significantly lower than in IR AL mice at 14 days and one month post-irradiation (Fig. 2Q–V). Oil red O staining further showed that the fat droplet area ratio was significantly higher in IR DR mice at all time points (Fig. 2W, X), suggesting that IR DR exacerbates the reduction of bone trabeculae area and fat droplet accumulation post-irradiation, which may underlie the inhibition of hematopoiesis.

#### Post-irradiation DR impairs regeneration capacity of HSCs

To determine the effect of DR on hematopoietic regeneration function per se post-irradiation, we performed BM transplantation experiments. BM cells from DR mice at one month post-irradiation were mixed with competitor BM cells at a 2:1 ratio and transplanted into recipient mice. Donor-derived cell chimerism was analyzed at different time points (1 month, 2 months, 3 months and 4 months) post-transplantation (Fig. 3A). We found that donor-derived cell chimerism was significantly lower in DR mice than in AL mice at all time points after primary transplantation (Fig. 3B–I). We further conducted a secondary transplantation experiment, and the results showed that BM from irradiated DR mice exhibited a poorer engraftment rate in the secondary transplantation (Fig. 3J, K). Further analysis revealed that the engraftment rates of PB B cells, T cells, and myeloid cells were also lower in irradiated DR mice compared to the AL group (Fig. 3L–Q), indicating that post-irradiation DR significantly impairs the regeneration capacity of BM hematopoietic cells per se.

#### Post-irradiation DR impairs DNA repair and leads to persistent DNA damage response in hematopoietic cells

Previous studies have shown that irradiation, even at low doses, can significantly activate the DNA damage signaling pathway in HSCs [38, 39], thereby affecting their hematopoietic function. To investigate the mechanism by which DR influences the hematopoietic function of HSCs post-irradiation, we first monitored the DNA damage signaling pathway in hematopoietic cells. Using qRT-PCR, we examined the expression of various genes involved in the DNA damage signaling pathway. We found that DR significantly upregulated the expression of DNA damage-related genes *Atm*, *Trp53*, *P21*, *Puma*, *Bax*, *caspase9* and *caspase3* in both total BM cells and HSPCs (Fig. 4A–E).

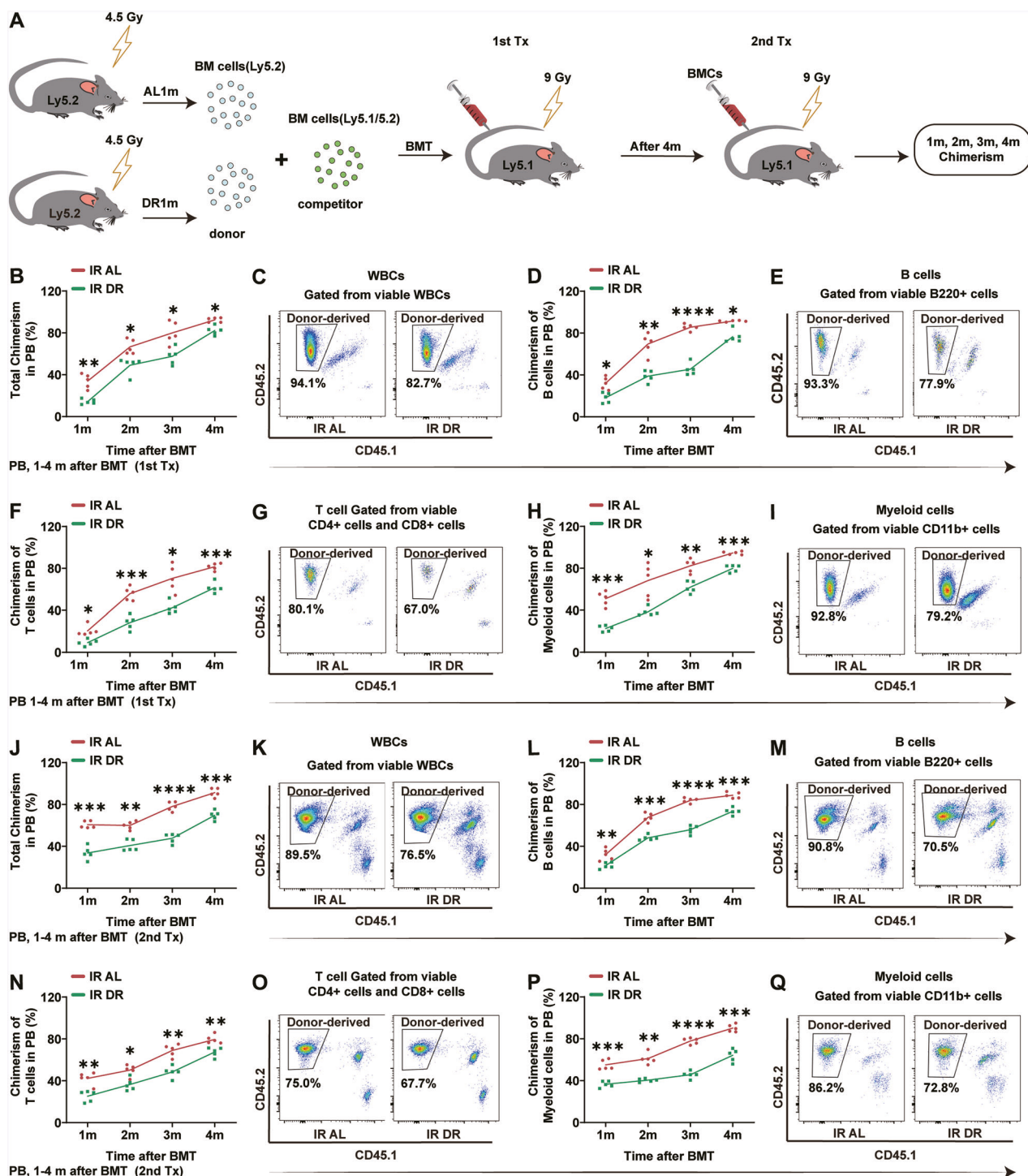
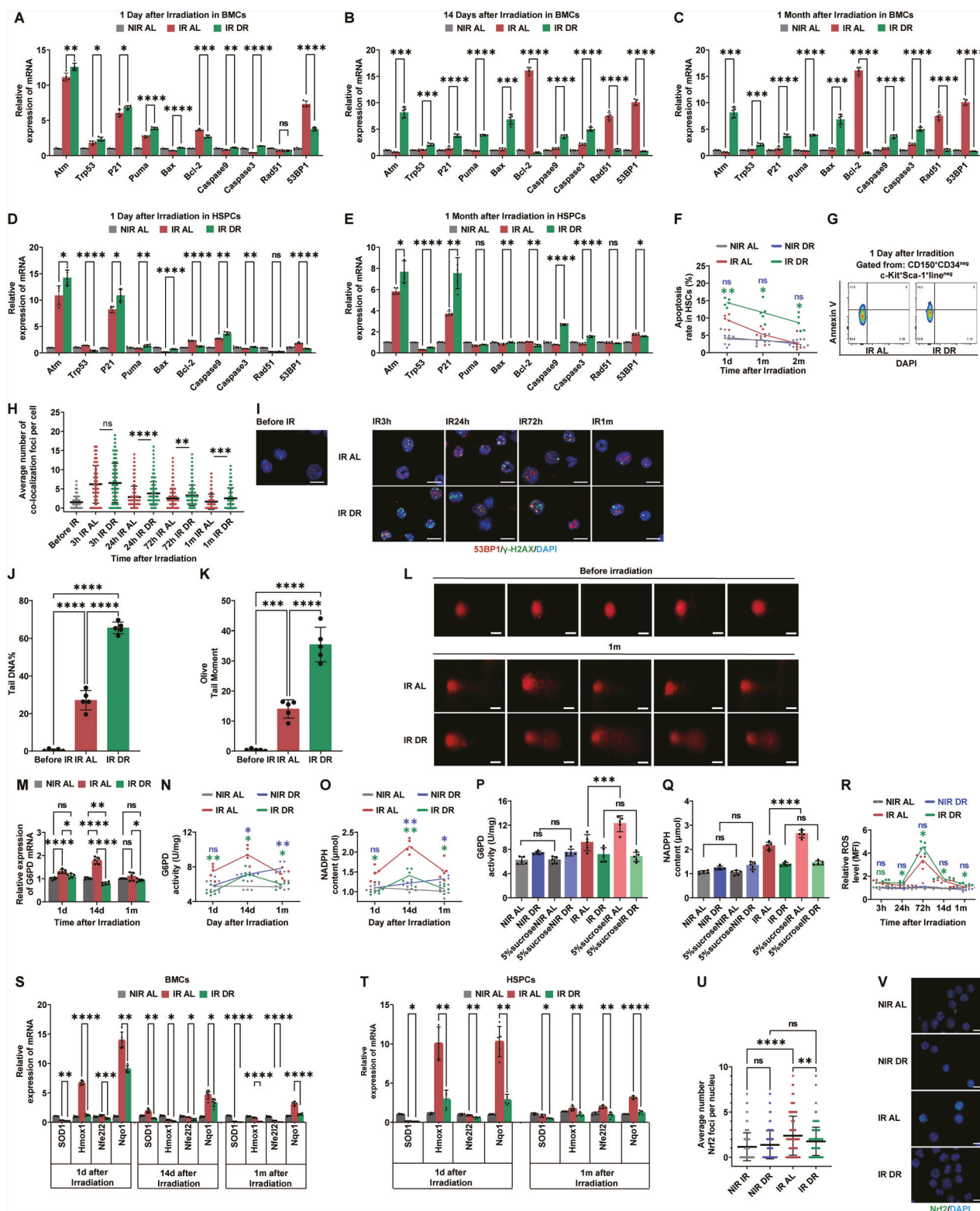


**Fig. 3 DR post-irradiation suppresses hematopoietic cell function in mice. A** Experimental scheme. Two-month-old wild-type C57BL/6 mice were subjected to 4.5 Gy X-ray irradiation and subsequently fed with an AL diet or DR diet for one month. Afterwards,  $2 \times 10^6$  BM cells from irradiated Ly5.2 donor mice were mixed with  $1 \times 10^6$  BM cells from Ly5.1/5.2 heterozygous competitor mice and primarily transplanted into lethally irradiated (9 Gy) Ly5.1 recipient mice for competitive BM transplantation. Four months after the primary transplantation,  $10 \times 10^6$  BM cells from the primary recipients were serially transplanted into lethally irradiated (9 Gy) Ly5.1 recipient mice. PB chimerism was analyzed at specified time points post-transplantation via FACS using blood collected from the retro-orbital sinus ( $n = 5$  mice per group from 1 experiment representative of 2 independent experiments). **B–I** Chimerism of donor-derived cells in the peripheral blood, including WBCs (B), B cells (D), T cells (F), and myeloid cells (H), after primary transplantation at the indicated time points. Representative FACS plot of WBCs (C), B cells (E), T cells (G), and myeloid cells (I) 4 months after primary transplantation. Chimerism of donor-derived cells in the PB, including WBCs (J), B cells (L), T cells (N), and myeloid cells (P), after secondary transplantation at the indicated time points. Representative FACS plot of WBCs (K), B cells (M), T cells (O), and myeloid cells (Q) 4 months after secondary transplantation. Results were displayed as mean  $\pm$  SD; ns, not significant; \* $p < 0.05$ ; \*\* $p < 0.01$ ; \*\*\* $p < 0.001$ ; \*\*\*\* $p < 0.0001$  by Two-way ANOVA test with Tukey's multiple comparisons test. BMT: bone marrow transplantation.



Concurrently, the expression of the anti-apoptotic signal molecule *Bcl-2* was downregulated (Fig. 4A–E). The primary forms of DNA damage induced by ionizing radiation include single-strand breaks (SSBs) and double-strand breaks (DSBs), sugar and base modifications, base oxidation damage, inter-strand crosslinks, DNA-protein crosslinks, and locally multiply damaged sites (LMDS) [40]. Among these, DSBs are considered

the most lethal form of DNA damage [27], as unrepaired or improperly repaired DSBs can lead to cell death or carcinogenesis, thereby affecting cell fate. DSBs are repaired by NHEJ or HR HSCs predominantly use non-homologous end joining (NHEJ) to repair DSBs caused by ionizing radiation [41, 42]. We further examined the expression of 53BP1 (p53 binding protein 1) and *Rad51* (Rad51 recombinase), molecules related to the DNA

**Fig. 4 Post-irradiation DR inhibits DNA repair and PPP and leads to persistent DNA damage response in hematopoietic cells. A–E** Mice were subjected to 4.5 Gy X-ray irradiation and subsequently fed with AL diet or DR diet. BM cells or c-Kit<sup>+</sup> HSPCs were harvested at the indicated time points for q RT-PCR analysis. NIR mice receiving an AL diet were monitored as a control. Relative expression of indicated genes involving DNA damage and repair were analyzed, with  $\beta$ -actin as the internal control ( $n = 5$  mice per group from 1 experiment representative of 2 independent experiments). **F, G** Apoptosis rates in HSCs at indicated time points post-irradiation and in NIR mice, as determined by FACS (F). Representative FACS plots at day 1 post-irradiation (G) ( $n = 5$  mice per group from 1 experiment, representative of 2 independent experiments). **H, I** Quantification and representative images of  $\gamma$ H2AX and 53BP1 colocalization in c-Kit<sup>+</sup> HSPCs at indicated time points post-irradiation and before irradiation, determined by immunofluorescent staining (scale bar: 10  $\mu$ m) ( $n = 5$  mice per group from 1 experiment representative of 2 independent experiments). **J–L** Quantification and representative images of comet assay tail DNA in c-Kit<sup>+</sup> HSPCs at indicated time points post-irradiation and before irradiation (scale bar: 10  $\mu$ m) ( $n = 5$  mice per group from 1 experiment, representative of 2 independent experiments). **M** Relative expression of G6PD mRNA in BM cells of AL and DR mice at the indicated time points post-irradiation and NIR AL mice, analyzed by qRT-PCR with  $\beta$ -actin as the internal control ( $n = 5$  mice per group from 1 experiment representative of 2 independent experiments). Dynamic measurements by ELISA of G6PD enzyme activity (N) and NADPH (O) content in BM cells of AL and DR mice at the indicated time points under IR or no-conditions conditions. **P** G6PD enzyme activity and **Q** NADPH content in BM cells of AL and DR mice given 5% sucrose water or normal drinking water at NIR/IR 14 days ( $n = 5$  mice per group from 1 experiment representative of 2 independent experiments). **R** Average fluorescence intensity of ROS in BM cells of AL and DR mice at indicated time points under non-irradiated or irradiated conditions ( $n = 5$  mice per group from 1 experiment representative of 2 independent experiments). Relative expression of indicated genes involving ROS in BM cells (S) and c-Kit<sup>+</sup> HSPCs (T) of AL and DR mice at indicated time points post-irradiation, analyzed by qRT-PCR with NIR AL mice as a control ( $n = 5$  mice per group from 1 experiment representative of 2 independent experiments). **U** and **V** Quantification and representative images of Nrf2 foci in the nucleus of BM cells of AL and DR mice at 5 h post-irradiation and under non-irradiated conditions, determined by immunofluorescent staining (scale bar: 10  $\mu$ m) ( $n = 5$  mice per group from 1 experiment representative of 2 independent experiments). Results were displayed as mean  $\pm$  SD; ns, not significant; \* $p < 0.05$ ; \*\* $p < 0.01$ ; \*\*\* $p < 0.001$ ; \*\*\*\* $p < 0.0001$  by one-way ANOVA test and Two-way ANOVA test with Tukey's multiple comparisons test. HSPCs: hematopoietic stem and progenitor cells. The purple symbols indicate statistical significance between the non-irradiated groups. The green symbols indicate statistical significance between the irradiated groups.

damage repair signaling pathway, by qRT-PCR. We found that DR significantly downregulated the expression of 53BP1, a key molecule in NHEJ, while the expression of *Rad51*, a gene involved in homologous recombination repair, was significantly downregulated in the early stages post-irradiation (Fig. 4A–E). Our experiments showed that DR significantly upregulated the DNA damage signaling pathway in irradiated hematopoietic cells, leading to sustained activation of DDR. The expression of 53BP1, which is involved in DNA damage repair, remained suppressed for extended periods post-irradiation. FACS analysis revealed that apoptosis in HSCs was consistently higher in DR mice compared to AL-fed irradiated mice, while it was similar in DR and AL NIR mice (Fig. 4F, G). Irradiation-induced DSBs trigger phosphorylation of H2AX at serine 139, forming  $\gamma$ H2AX foci. In response to IR, 53BP1 becomes hyperphosphorylated and colocalizes with  $\gamma$ H2AX, participating in protein recruitment, signal transduction, and repair pathway choice, making simultaneous detection of  $\gamma$ H2AX and 53BP1 colocalization an effective approach for analyzing DSB formation and repair [43]. To elucidate the effect of DR on DNA damage and its repair in hematopoietic cells, we sorted c-Kit<sup>+</sup> hematopoietic cells and performed immunofluorescence staining for  $\gamma$ -H2AX and 53BP1 colocalization and counting at different time points post-irradiation (Fig. 4H, I).  $\gamma$ H2AX and 53BP1 colocalization was hardly detectable in NIR mice (Fig. 4H, I). Both the AL and DR groups showed upregulated  $\gamma$ H2AX and 53BP1 colocalization at the early time point (3 h) post-irradiation. However,  $\gamma$ H2AX and 53BP1 colocalization significantly decreased in AL mice 24 h after irradiation, while they remained elevated in DR mice. At 72 h,  $\gamma$ H2AX and 53BP1 colocalization further decreased in AL mice but stayed high in DR mice. Throughout the early time points and up to 72 h,  $\gamma$ H2AX and 53BP1 colocalization was consistently higher in DR mice. After one month,  $\gamma$ H2AX and 53BP1 colocalization in AL mice had significantly decreased to about one foci per cell, whereas DR mice still exhibited approximately two foci per cell, indicating inhibited DNA damage repair due to DR. This suggests that post-irradiation DR significantly suppresses DNA damage repair. We further assessed DNA damage in hematopoietic cells one month post-irradiation using the Comet assay, which also showed that DR mice exhibited significantly higher levels of DNA damage comparing to AL mice (Fig. 4J–L). In NIR mice, tail DNA and

Olive tail moment were at extremely low levels (Fig. 4J–L). These results indicate that DR significantly suppresses DNA damage repair after irradiation in hematopoietic cells.

#### Post-irradiation DR significantly inhibits PPP in hematopoietic cells

The above experimental results indicate that post-irradiation DR significantly suppresses DNA damage repair in hematopoietic cells. To further investigate the underlying mechanisms, we examined the PPP. Recent studies have shown that DR under homeostatic conditions can significantly inhibit the glycolytic metabolic pathway in hematopoietic cells [44]. The PPP synthesizes the pentose phosphates required for DNA synthesis during DNA damage repair. The PPP is another major pathway for glucose metabolism. Radiation exposure directly causes DNA damage and also generates a large amount of ROS, which can further lead to DNA damage [45]. NADPH produced by the PPP is crucial for combating ROS and repairing ROS-induced damage [46]. Additionally, the PPP provides the necessary precursor R5P for DNA damage repair [47]. We studied the regulatory effect of post-irradiation DR on the PPP.

Firstly, we performed qRT-PCR to detect the expression of G6PD in BM cells of DR mice at different time points post-irradiation (Fig. 4M). G6PD is the rate-limiting enzyme of the PPP, catalyzing the conversion of glucose-6-phosphate to 6-phosphoglucono- $\delta$ -lactone, which is the first and rate-limiting step of the PPP. We found that post-irradiation, the expression of G6PD was significantly upregulated in the BM cells of AL mice, whereas it was not upregulated and was significantly lower in DR mice compared to AL mice (Fig. 4M). This strong inhibitory effect on G6PD expression by DR was observed at 1 day, 14 days, and one month post-irradiation, with the most pronounced effect at 14 days (Fig. 4M). We further measured G6PD enzyme activity using an ELISA method (Fig. 4N). Similarly, at 1 day, 14 days, and one month post-irradiation, G6PD activity in DR mice was significantly lower than in AL mice. NADPH, a major product of the PPP, primarily originates from the PPP and reflects its activity. Therefore, we further assessed NADPH levels to validate the expression regulation of the PPP in whole BM cells post-irradiation and the effect of DR (Fig. 4O). We found that NADPH levels were significantly lower in DR mice compared to AL mice at 1 day, 14 days, and one month post-irradiation (Fig. 4O). These findings

indicate that on 14 days post-irradiation, DR significantly inhibits the PPP in BM hematopoietic cells. Interestingly, in the IR group of mice, we observed that although there was no significant difference in G6PD enzyme activity and NADPH levels between the AL and DR groups at day 3, at days 14 and 30, the NIR DR mice exhibited higher G6PD enzyme activity and NADPH levels compared to the AL group (Fig. 4N, O).

To further investigate the effect on the PPP by DR, we provided mice with high-glucose drinking water and measured G6PD and NADPH levels after 14 days (Fig. 4P, Q). In irradiated AL mice, high glucose further increased G6PD enzyme activity and NADPH levels. However, in irradiated DR mice, there was no significant upregulation of G6PD activity or NADPH levels even after high-glucose supplementation, indicating that DR significantly inhibits PPP activation post-irradiation. However, in the NIR mice, a high-sugar diet did not significantly increase G6PD enzyme activity or NADPH levels in either the AL or DR groups (Fig. 4P, Q).

We also measured the relative fluorescence intensity of ROS using FACS, finding that DR mice had consistently higher ROS levels compared to AL mice at the one-month time point (Fig. 4R). Additionally, qRT-PCR analysis of antioxidant gene expression in BM cells and c-Kit<sup>+</sup> cells revealed that *SOD1*, *Hmox1*, *Nfe2l2* and *Nqo1* gene expression levels were consistently lower in DR mice compared to AL mice at the one-month time point (Fig. 4S, T). This indicates that DR significantly increases ROS levels and reduces ROS scavenging. When intracellular ROS levels increase (e.g., during oxidative stress), the critical cysteine residues in Keap1 are oxidized or modified, leading to the release of Nrf2 from the Keap1 complex, thereby escaping degradation and translocating into the nucleus [48, 49]. Nrf2 plays a pivotal role in responding to oxidative stress (elevated ROS), inflammation, toxins, and radiation [50]. We assessed Nrf2 expression using immunofluorescence staining. In the NIR groups, both AL and DR mice exhibited extremely low levels of Nrf2 expression, with no significant difference between the two groups (Fig. 4U, V). However, at 5 hours post-irradiation, a marked increase in Nrf2 nuclear translocation and expression was observed in AL mice (Fig. 4U, V), whereas DR mice showed no significant upregulation of Nrf2 or nuclear translocation (Fig. 4U, V). A comparison between the irradiated AL and DR groups revealed that Nrf2 expression levels in DR mice were significantly lower than those in AL mice (Fig. 4U, V). These findings suggest that DR treatment significantly suppresses Nrf2 upregulation and nuclear translocation following irradiation, thereby impairing the activation of the antioxidant stress pathway and preventing effective ROS clearance.

#### Down-regulation of the PPP impairs hematopoiesis in AL mice post-irradiation

To further validate the impact of the PPP on DNA repair and hematopoietic function in irradiated hematopoietic cells, we administered 6-AN injections to AL mice post-irradiation (Fig. 5A). 6-AN is a PPP inhibitor that, once captured in mammalian cells, is converted by NAD(P) glycohydrolase to the non-reducible forms 6-ANAD and 6-ANADP, with 6-ANADP being a strong competitive inhibitor of G6PD [51, 52]. We administered 6-AN immediately after irradiation, while control mice received saline injections. The injections were continued for seven consecutive days. One month later, we harvested the total BM cells to measure G6PD enzyme activity and NADPH levels. The 6-AN injections significantly reduced G6PD activity and NADPH levels in the BM cells of AL mice (Fig. 5B, C). Interestingly, we observed that post-irradiation 6-AN administration significantly decreased PB WBCs, neutrophils, and lymphocytes (Fig. 5D–F). Additionally, the weights of the spleen and thymus were significantly reduced in the 6-AN group (Fig. 5G, H). The total number of BM cells was markedly lower in the 6-AN injection

group compared to the control group (Fig. 5I). Further FACS analysis showed a significant decrease in the frequencies of B cells in the PB, spleen and BM of the 6-AN group (Fig. 5J–L). The frequencies of HSCs and progenitor cells, including CMPs and GMPs, were also significantly reduced in the 6-AN group (Fig. 5M–Q). We further assessed the effect of PPP inhibition on DNA damage repair using immunofluorescence staining for γ-H2AX and 53BP1 colocalization. We found that the number of γ-H2AX and 53BP1 colocalization in the BM of the 6-AN group was significantly higher than in the saline-injected control group, indicating that 6-AN inhibits DNA damage repair (Fig. 5R, S). To explore the effect of PPP inhibition and DNA damage repair suppression on hematopoietic function, we harvested whole BM cells from the mice at the one-month time point and performed hematopoietic cell competitive transplantation. We assessed donor-derived chimerism at different time points post-transplantation. The chimerism of donor-derived cells, including total chimerism, B cells, T cells, and myeloid cells, was significantly lower in the 6-AN group compared to the saline-injected control group (Fig. 5T–A'). These results further demonstrate that inhibiting the PPP with 6-AN impairs the hematopoietic cell reconstitution capacity in irradiated AL mice.

#### UP-regulation of the PPP rescues hematopoiesis in post-irradiation DR mice

To further elucidate the regulatory role of PPP in DR mice post-irradiation, we activated PPP using the activator AG1 in DR mice post-irradiation (Fig. 6A). G6PD is functionally active in dimeric or tetrameric forms. AG1 promotes the formation and stabilization of G6PD dimers, thereby enhancing G6PD activation [53, 54]. In vivo experiments in mice have confirmed the stimulatory effect of AG1 on PPP [53, 54]. We first confirmed successful activation of PPP by detecting increased G6PD enzyme activity and NADPH levels in BM cells of DR mice by AG1 injection (Fig. 6B, C). AG1 administration also significantly improved hematopoietic parameters, including WBC, neutrophil, and lymphocyte counts in PB (Fig. 6D–F). Additionally, spleen and thymus weights were significantly higher in AG1-treated mice compared to the control group (Fig. 6G, H). The total BM cell count was increased in the AG1 injection group (Fig. 6I). FACS analysis revealed that the frequencies of B cells in the PB, spleen and BM were significantly higher in the AG1 group compared to the DMSO group (Fig. 6J–L). Additionally, the frequencies of HSCs, CMPs, and GMPs were also significantly higher in the AG1 group compared to the DMSO control group (Fig. 6M–Q). These experiments indicate that activating the PPP with AG1 in post-irradiation DR mice can promote hematopoietic regeneration.

We further investigated the effect of AG1 on DNA damage repair in hematopoietic cells. Immunofluorescence staining for γ-H2AX and 53BP1 colocalization showed that the number of γ-H2AX and 53BP1 colocalized foci in BM cells was significantly reduced in the AG1 injection group (Fig. 6R, S), suggesting that AG1 activation of the PPP can significantly improve DNA damage repair in hematopoietic cells of post-irradiation dietary-restricted mice. To further clarify its impact on hematopoietic reconstitution, we transplanted BM cells from one-month-old mice with competitor cells into recipient mice. We found that the hematopoietic reconstitution capacity of the AG1 activation group was significantly higher than that of the DMSO control group (Fig. 6T–A'). The total chimerism, B cell chimerism, T cell chimerism, and myeloid cell chimerism in the PB of the AG1 group were significantly higher than those in the DMSO group (Fig. 6T–A'). These experiments indicate that upregulating the PPP with AG1 significantly improves DNA damage repair and promotes hematopoietic reconstitution in hematopoietic cells of post-irradiation DR mice.

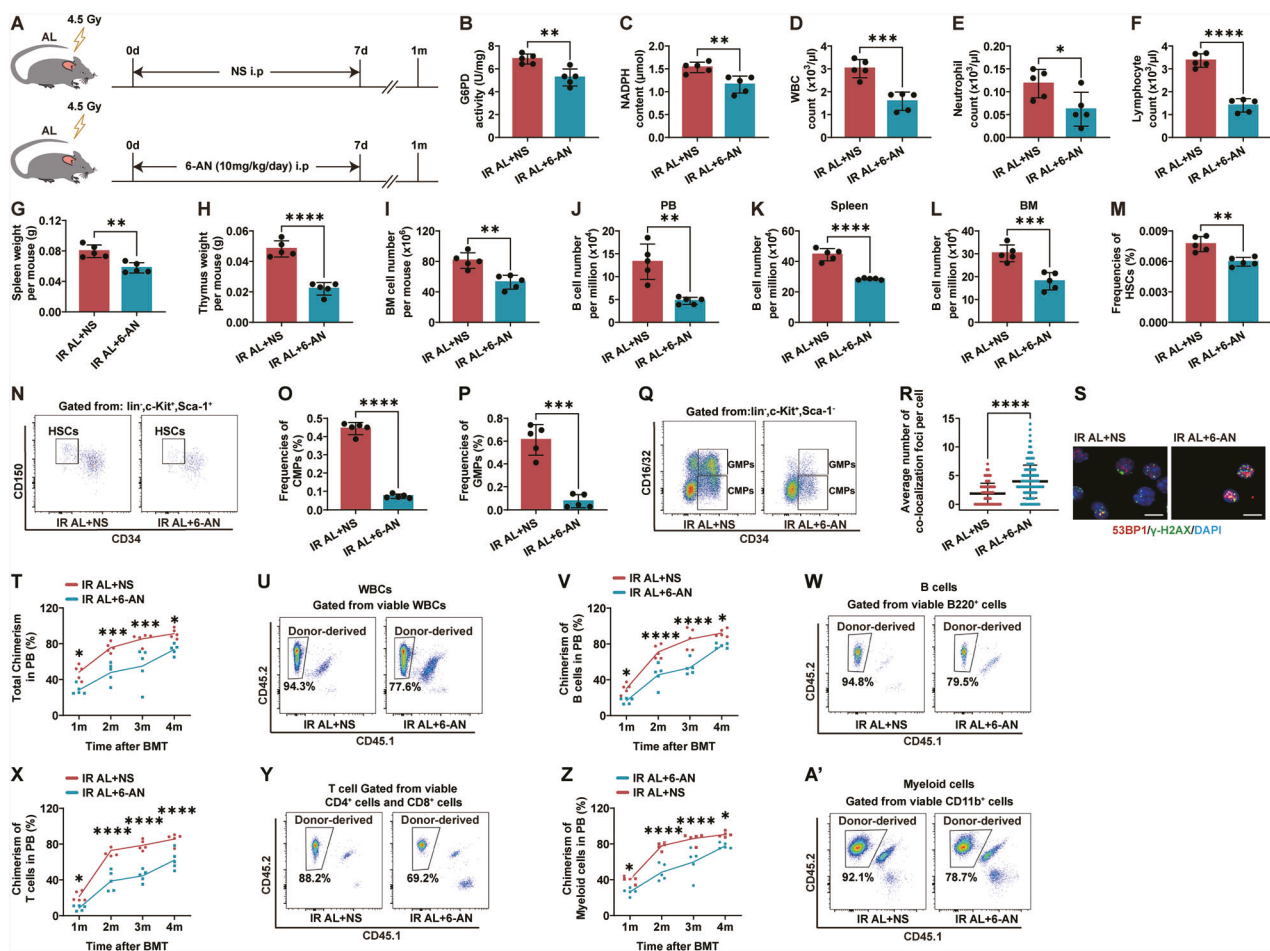


**Fig. 5 Inhibition of the PPP suppresses the hematopoietic system in irradiated mice.** **A** Experimental scheme. Wild-type C57BL/6 mice (2 months old) were irradiated with 4.5 Gy X-rays and fed with an AL diet. Mice were then injected intraperitoneally with 10 mg/kg/day of 6-aminonicotinamide (6-AN) or saline daily for 7 days post-irradiation, and were continued on an AL diet until 1 month post-irradiation ( $n = 5$  mice per group from 1 experiment representative of 2 independent experiments). G6PD enzyme activity (**B**) and NADPH content (**C**) in BM cells of AL mice 1 month post-irradiation, analyzed using ELISA. WBC (**D**), Neutrophil (**E**), and lymphocyte (**F**) counts in PB of AL mice 1 month post-irradiation. **G**, **H** Spleen and thymus weights of AL mice 1 month post-irradiation. **I** Total BM cell counts of AL mice 1 month post-irradiation. **J** FACS analysis of frequencies of B220<sup>+</sup> lymphocytes in PB (**J**), spleen (**K**), BM (**L**); and frequencies of HSCs (**M**), CMPs (**O**), and GMPs (**P**), and representative FACS Plots of HSCs (**N**) and CMPs/GMPs/MEPs (**Q**) of AL mice 1 month post-irradiation. **R** and **S** Quantification and representative images of  $\gamma$ H2AX and 53BP1 colocalization in BM cells of AL mice 1 month post-irradiation, determined by immunofluorescent staining (scale bar: 10  $\mu$ m). **T–A'** Chimerism of donor-derived cells in the PB, including WBCs (**T**), B cells (**V**), T cells (**X**), and myeloid cells (**Z**) chimerism after transplantation at indicated time points and representative FACS plot of WBCs (**U**), B cells (**W**), T cells (**Y**), myeloid cells (**A'**) at 4 months post-transplantation. Results were displayed as mean  $\pm$  SD; ns, not significant; \* $p < 0.05$ ; \*\* $p < 0.01$ ; \*\*\* $p < 0.001$ ; \*\*\*\* $p < 0.0001$  by unpaired two-tailed Student's *t*-test and Two-way ANOVA test with Tukey's multiple comparisons test. IR AL + 6-AN: irradiated ad libitum group injected with 6-AN; IR AL + NS: irradiated ad libitum group injected with saline.

### Post-irradiation DR followed by RF significantly promotes hematopoiesis

To further examine the effects of refeeding (RF) on DNA repair and hematopoietic function after irradiation, mice were subjected to DR for one week, followed by three weeks of AL feeding (Fig. 7A). RF significantly increased G6PD activity and NADPH levels in BM cells (Fig. 7B and C). At one month post-irradiation, RF mice exhibited higher WBC, neutrophil, and lymphocyte counts than DR mice, comparable to AL controls, while RBC and platelet counts were unaffected (Fig. 7D–H). Spleen and thymus weights and total BM cell count were significantly elevated in RF mice (Fig. 7I–K). Flow cytometric analysis revealed increased frequencies of B cells, HSCs, CMPs, GMPs, and BMRMs, but not MEPs, in RF mice compared with DR mice (Fig. 7L–S). HSC apoptosis was reduced in RF mice to levels similar to AL controls (Fig. 7T), and ROS levels were lower than in DR mice (Fig. 7U). Immunofluorescence staining for  $\gamma$ -H2AX and 53BP1 colocalization showed fewer colocalized foci in RF BM cells than in DR mice, indicating

enhanced DNA repair (Fig. 7V and W). These results indicate that short-term DR following radiation exposure can induce hematopoietic suppression and an increase in DNA damage, but these phenotypes can be reversed upon resumption of ad libitum feeding.

### Severe neutropenia negatively relates to BMI in patients receiving pelvic radiotherapy

In order to further study the role of post-irradiation nutritional status on hematopoietic cell counts in patients, we retrospectively collected routine blood counts from 101 patients who received radiotherapy for pelvic cancer at our centre from 2021/10/18 to 2023/6/30. These patients underwent weekly hematological monitoring during radiotherapy, and we recorded WBC, neutrophil, lymphocyte, RBC, and platelet counts, as well as the patients' BMI (Fig. 8A–E). We found that patients with WBC counts  $\leq 2 \times 10^3/\mu\text{L}$  the BMI values were significantly lower than those with WBC counts never  $< 2 \times 10^3/\mu\text{L}$  (Fig. 8A). We compared the data of

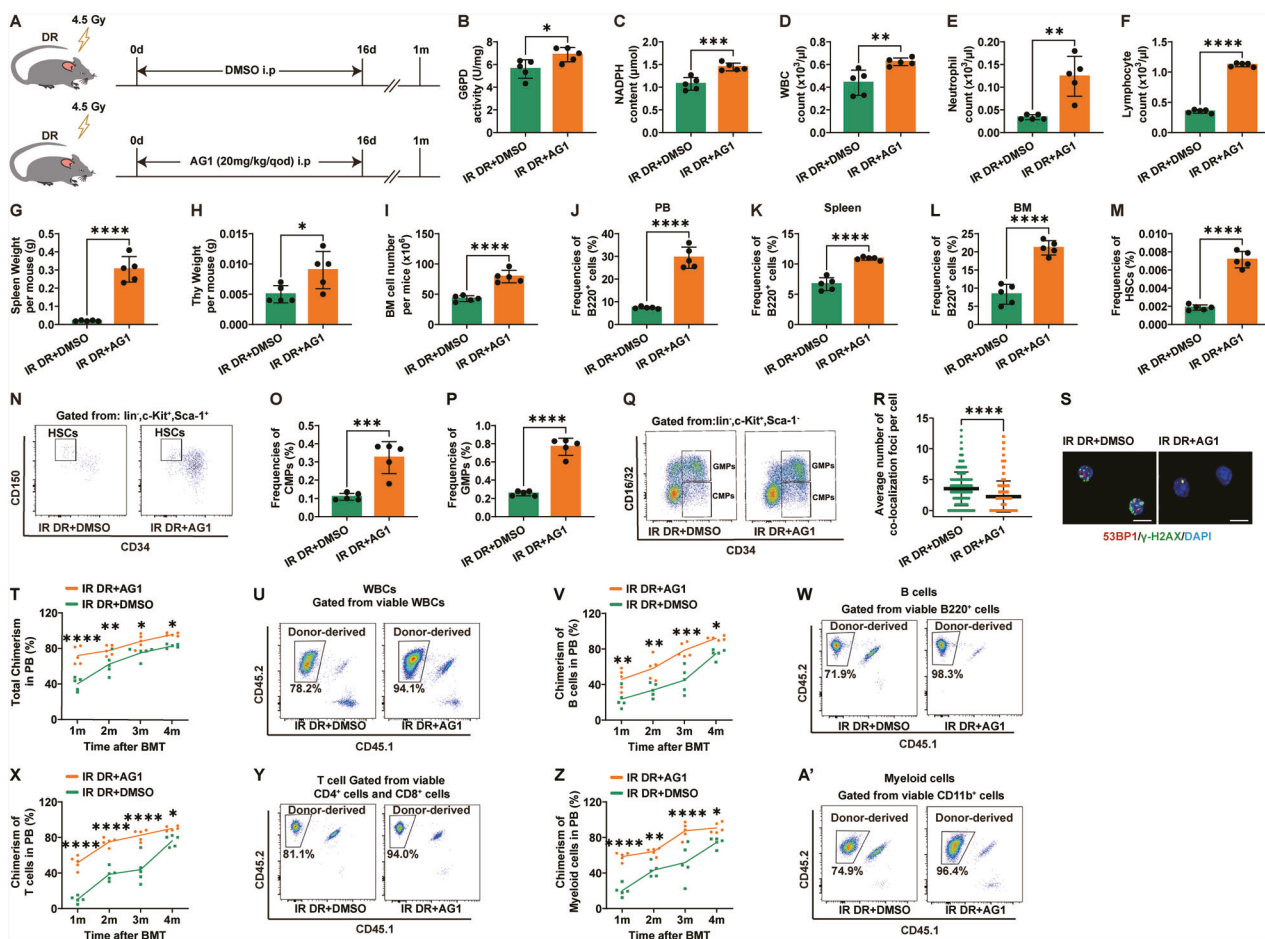


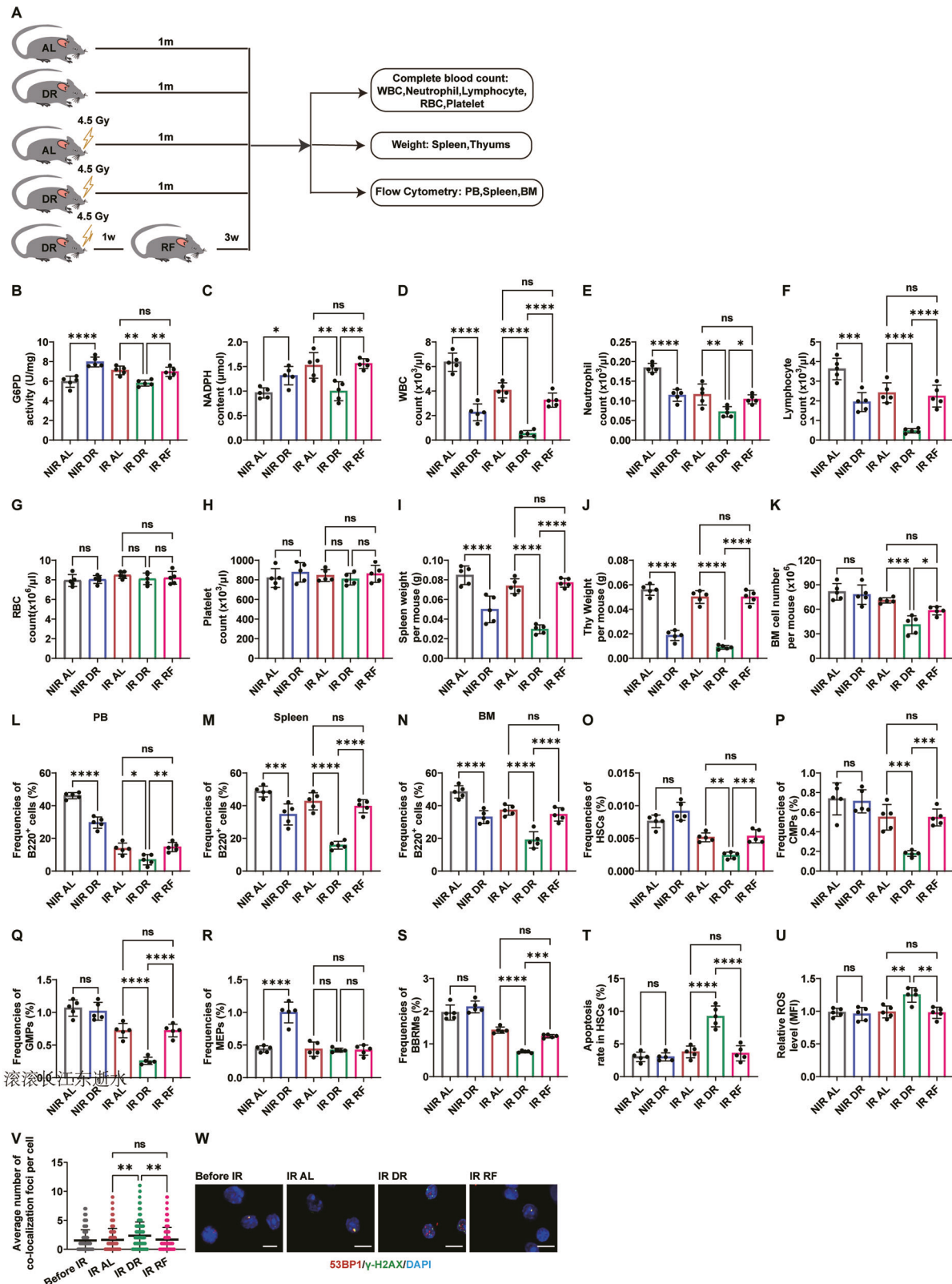
**Fig. 6 Activation of the PPP improves hematopoietic function in dietary-restricted (DR) mice post-irradiation.** **A** Experimental scheme. Wild-type C57BL/6 mice (2 months old) were irradiated with 4.5 Gy X-rays, fed with a DR diet. Mice were then injected intraperitoneally with 20 mg/kg of AG1 or DMSO every other day for 9 times post-irradiation, and were continued on DR until 1 month post-irradiation ( $n = 5$  mice per group from 1 experiment representative of 2 independent experiments). G6PD enzyme activity (**B**) and NADPH content (**C**) in BM cells of DR mice 1 month post-irradiation, analyzed using ELISA. WBC (**D**), Neutrophil (**E**), and lymphocyte (**F**) counts in PB of DR mice 1 month post-irradiation. **G, H** Spleen and thymus weights of DR mice 1 month post-irradiation. **I** Total BM cell counts of DR mice 1 month post-irradiation. FACS analysis of frequencies of B220<sup>+</sup> lymphocytes in PB (**J**), spleen (**K**), BM (**L**); and frequencies of HSCs (**M**), CMPs (**O**) and GMPs (**P**), and representative FACS Plots of HSCs (**N**) and CMPs/GMPs/MEPs (**Q**) of DR mice 1 month post-irradiation. **R** and **S** Quantification and representative images of  $\gamma$ H2AX and 53BP1 colocalization in BM cells of DR mice 1 month post-irradiation, determined by immunofluorescent staining (scale bar: 10  $\mu$ m). Chimerism of donor-derived cells in the PB, including WBCs (**T**), B cells (**V**), T cells (**X**), and myeloid cells (**Z**) chimerism after transplantation at indicated time points and representative FACS plot of WBCs (**U**), B cells (**W**), T cells (**Y**), myeloid cells (**A'**) at 4 month post-transplantation. Results were displayed as mean  $\pm$  SD; ns, not significant; \* $p < 0.05$ ; \*\* $p < 0.01$ ; \*\*\* $p < 0.001$ ; \*\*\*\* $p < 0.0001$  by unpaired two-tailed Student's *t* test, and Two-way ANOVA test with Tukey's multiple comparisons test. IR DR + AG1: irradiated dietary restriction group injected with AG1; IR DR + DMSO: irradiated dietary restriction group injected with DMSO.

patients who experienced the most severe neutropenia (grade 3–4) with those who either never experienced neutropenia or only experienced grade <3 toxicity. Similarly for patients with grade 3–4 neutropenia had significantly lower BMI values compared to those who never experienced grade 3 or higher neutropenia (Fig. 8B). In lymphocyte counts it was also found that patients presenting with lymphocytes  $\leq 0.8 \times 10^3/\mu\text{L}$  had significantly lower BMI than patients with lymphocyte counts never  $< 0.8 \times 10^3/\mu\text{L}$  (Fig. 8C). As for platelet as well as RBC counts, there was no significant difference in BMI values between patients with platelets  $\leq 100 \times 10^3/\mu\text{L}$  or  $> 100 \times 10^3/\mu\text{L}$ , or between patients with and without RBC reduction (Fig. 8D, E). Next, we performed the ROC test on the BMI after grouping the WBC, neutrophil and lymphocyte counts, which differed in the random test, and plotted the ROC curve, and calculated the Youden index to be 21.59 for WBCs, 21.06 for neutrophil, and 20.73 for lymphocytes (Fig. 8F). The results indicated that the degree of myelosuppression after irradiation and the BMI were related. Based on the Youden index

calculated from the ROC curve, patients were divided into two groups: BMI  $\geq 22$  (high BMI group) and BMI  $< 22$  (low BMI group). The basic characteristics of the patients were presented in Supplementary Table 3. A comparison of the BW dose between the two groups revealed no statistically significant difference (Fig. 8G).

## DISCUSSION

Radiation therapy remains one of the main treatments for tumors. However, radiotherapy often involves the pelvis, flat bones, and long bones [55], which are hematopoietic tissues. Even low doses of radiation can cause significant damage to these tissues and reduce blood cell counts [27]. Therefore, hematological toxicity is one of the most common complications of radiotherapy. Severe reductions in WBCs [4] or platelets [56] due to radiotherapy can even lead to treatment interruptions, affecting the overall efficacy and prognosis of anti-tumor treatment. Although numerous



studies have demonstrated the negative impact of radiation on hematopoiesis [56, 57], the factors causing severe hematopoietic dysfunction in some patients remain unclear. Our study is the first to propose that food reduction post-irradiation can significantly inhibit hematopoiesis.

We are the first to propose that DR post-irradiation can cause hematopoietic cells to remain at persistently low levels with significantly delayed recovery. BM transplantation experiments further confirmed significant impairment of HSC function. We provide the first experimental evidence that DR post-irradiation

**Fig. 7 Suppression of hematopoiesis in mice by RF post-irradiation.** **A** Experimental scheme. Wild-type C57BL/6 mice (2 months old) were irradiated with 4.5 Gy X-rays, fed with either AL diet or DR diet or DR diet 1 week, then AL feeding 3 weeks (daily food intake restricted to 70% of the intake of age- and sex-matched AL mice). NIR mice receiving an AL or DR diet were also monitored as a control ( $n = 5$  mice per group from 1 experiment representative of 2 independent experiments). **B** and **C** G6PD enzyme activity (**B**) and NADPH content (**C**) in BM cells of RF mice 1 month post-irradiation, analyzed using ELISA. WBC (**D**), Neutrophil (**E**), and lymphocyte (**F**), RBC (**G**), platelet (**H**) counts in PB of RF mice 1 month post-irradiation. **I**, **J** Spleen and thymus weights of RF mice 1 month post-irradiation. **K** Total BM cell counts of RF mice 1 month post-irradiation. FACS analysis of frequencies of B220<sup>+</sup> lymphocytes in PB (**L**), spleen (**M**), BM (**N**); and frequencies of HSCs (**O**), CMPs (**P**) and GMPs (**Q**), MEPs (**R**), and RMBMs (**S**) of RF mice 1 month post-irradiation. **T** Apoptosis rates in HSCs of RF mice 1 month post-irradiation. **U** Average fluorescence intensity of ROS in BM cells of RF mice 1 month post-irradiation. **V** and **W** Quantification and representative images of  $\gamma$ -H2AX and 53BP1 colocalization in BM cells of RF mice 1 month post-irradiation, determined by immunofluorescent staining (scale bar: 10  $\mu$ m). Results were displayed as mean  $\pm$  SD; ns, not significant; \* $p$  < 0.05; \*\* $p$  < 0.01; \*\*\* $p$  < 0.001; \*\*\*\* $p$  < 0.0001 by one-way ANOVA test with Tukey's multiple comparisons test. IR: RF: irradiated refeeding group.

can significantly inhibit the activation of PPP in hematopoietic cells, reduce NADPH, thereby inhibiting DNA damage repair and reducing ROS antioxidation. Activating PPP in DR mice can significantly improve HSC function, allowing hematopoiesis to recover, while inhibiting PPP in AL mice, the effects of DR impairing hematopoiesis. Therefore, we mechanistically show that DR post-irradiation impairs DNA damage repair and regeneration capacity of HSCs through downregulation of the PPP, which produces NADPH that plays a crucial role in mitigating ROS [45] and provides necessary 5-phosphoribose for DNA damage repair [58].

Clinically, we found that patients with lower BMI and poorer nutritional status are more likely to experience severe reductions in WBCs, neutrophils, and lymphocytes during pelvic radiotherapy. This is the first clinical proof of a clear correlation between nutritional status and hematological toxicity of radiotherapy. Our study identifies a new mechanism for radiotherapy-induced hematological toxicity and confirms the crucial role of nutritional intake in post-radiation hematopoiesis. Notably, in the clinical setting, patients receiving radiotherapy often undergo concurrent chemotherapy, and radiotherapy itself is usually delivered in fractionated doses over an extended course (for example, standard long-course radiotherapy for rectal cancer lasts approximately five weeks). Moreover, given that patients typically undergo continuous anti-tumor treatment, reductions in dietary intake often persist for several weeks to months, or even longer. In the current study, we investigated the effects of DR lasting up to 2 months on hematopoiesis, which can well reflect the actual clinical situation, and thus may have important clinical implications. The current study indicates a potential role of nutritional status on DNA damage repair and ROS levels through regulation of the PPP, and consequently affecting HSCs and hematopoiesis. The study draws attention to maintaining good nutritional status and dietary intake for patients undergoing radiotherapy to reduce hematopoietic toxicities, so as to ensure continuation of radiotherapy and subsequent treatments, thereby improving the prognosis.

Although the clinical observation of hematologic toxicity related to radiotherapy has been recognized for a long time [1, 2], research into its mechanisms has so far primarily focused on the direct damage to hematopoietic cells caused by radiation, as well as technical modifications in radiotherapy, such as Stereotactic Body Radiotherapy (SBRT) [59] or pelvic (active) BM sparing radiotherapy [60], to minimize the radiation dose to hematopoietic tissues. However, there has been a lack of research on other factors beyond radiation exposure, such as patient-specific factors that might influence hematopoiesis. Our study is the first to identify a clear correlation between a patient's dietary and nutritional status and radiotherapy-related hematologic toxicity. In this study, we observed that DR following irradiation reduced PB WBCs, neutrophils, and lymphocytes, whereas RBC and platelet counts appeared largely unaffected. Consistent with our previous findings that DR enhanced HSC differentiation toward the megakaryocyte-erythroid lineage under steady-state conditions,

these results suggested that while irradiation exerted suppressive effects on erythropoiesis, the intrinsic stimulatory influence of DR on HSC lineage commitment may have partially compensated for radiation-induced inhibition. This interplay could explain why erythropoiesis remained largely comparable between DR and AL groups despite the stress of irradiation. The current study found that DR following radiation exposure can regulate both HSPCs and the BM environment, thereby inhibiting hematopoiesis after radiation exposure.

Radiation exposure leads to significant DNA damage in hematopoietic cells [2, 57], activating the DDR signaling pathway [39], which is one of the primary reasons for radiation-induced impairment of HSC function. This study found that compared to AL, DR can further upregulate genes related to the DDR signaling pathway, including *Atm*, *P53*, *P21*, *Puma*, *Bax*, *Caspase9*, and *Caspase3*, while downregulating the expression of the anti-apoptotic signal molecule *Bcl-2*. This regulation of gene expression was observed in both total BM cells and HSPCs. Activation of the DDR signaling pathway simultaneously initiates the DNA damage repair system [38], where the repair of DNA damage in hematopoietic cells can occur through both HR and NHEJ [27]. Among these, NHEJ is the more commonly used repair mechanism in HSPCs [41, 42]. *Rad51* and *53BP1* are key molecules in the HR and NHEJ pathways [41, 61], respectively. Our study found that in irradiated HSPCs of DR mice, the upregulation levels of *Rad51* and *53BP1* were significantly lower than those in AL mice. Using  $\gamma$ -H2AX and 53BP1 colocalized staining and comet assays, we observed a significant delay in DNA damage repair in the HSPCs of DR mice after IR. These findings suggest that DR after radiation exposure inhibits DNA damage repair in the HSPCs of mice, leading to sustained activation of the DDR system and thereby impairing their hematopoietic function.  $\gamma$ -H2AX and 53BP1 colocalized staining and comet assays were performed on c-Kit<sup>+</sup> cells, which include proliferative cells (more differentiated progenitors) and quiescent cells (HSCs and less differentiated progenitors). The proportion of HSCs is very low compared to progenitors, so the damaged cells are likely to be almost exclusively progenitors. In BM transplantation experiments, when we transplanted hematopoietic cells from irradiated, DR mice into recipients, the HSCs from the irradiated DR donors showed significantly reduced hematopoietic reconstitution capacity, even though the recipients were fed AL. This further confirms that DR post-irradiation can intrinsically impair the regeneration function of HSCs.

We further explored the mechanism by which DR post-irradiation significantly inhibits DNA damage repair in hematopoietic cells. Previous studies have shown that IR directly causes DNA damage and generates a significant amount of ROS, which can further exacerbate DNA damage [62]. The NADPH produced by PPP is crucial for combating ROS and repairing ROS-induced damage [45]. Additionally, the PPP provides the necessary precursor, R5P, for DNA damage repair [46, 47, 63]. Transgenic mice overexpressing G6PD have been shown to reduce ROS accumulation in multiple systems during aging, thereby extending

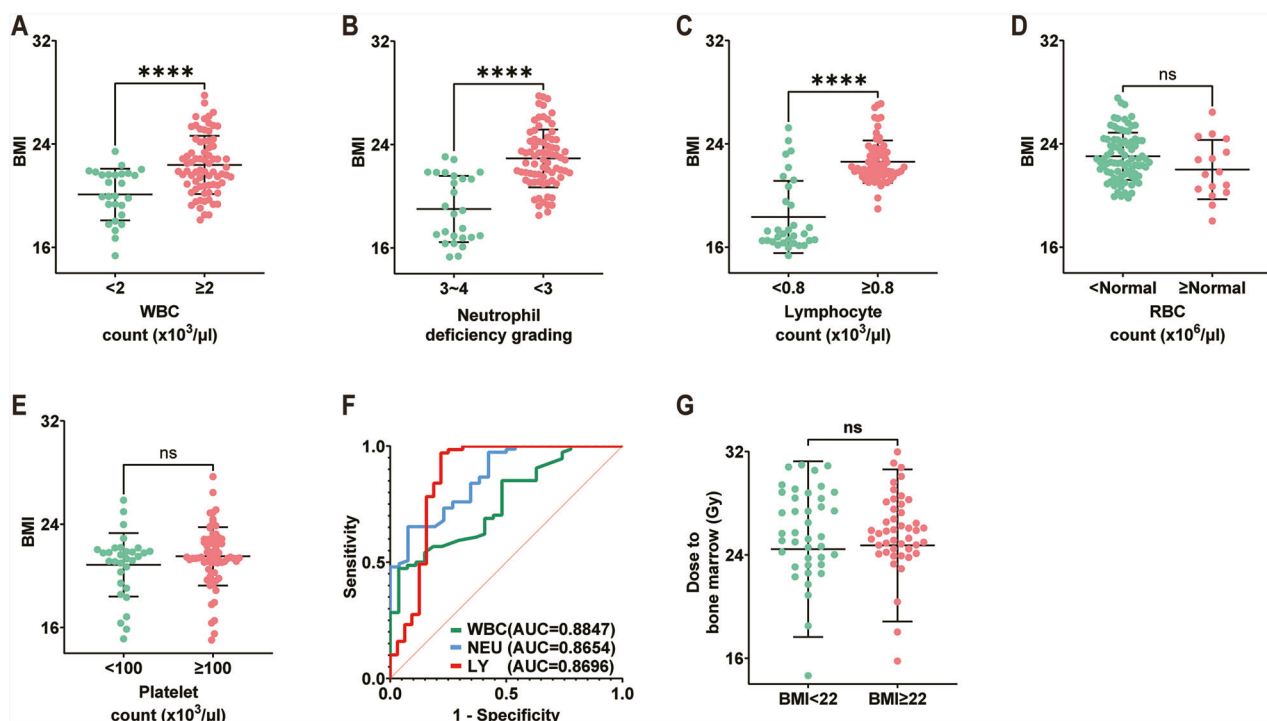


**Fig. 8 Lower-weight individuals are more likely to have haematopoietic damage after pelvic radiotherapy.** Height and weight were measured weekly in 101 patients undergoing pelvic radiotherapy, and BMI was calculated by taking the mean of the BMI values of the same patient. The values of PB neutrophil, WBC, lymphocyte, RBC, and platelet counts of the patients were recorded weekly for one month after radiotherapy. **A** Those with a WBC count  $\leq 2 \times 10^3/\mu\text{L}$  had a smaller BMI than those with a WBC count  $> 2 \times 10^3/\mu\text{L}$ . **B** Those with neutrophil deficiencies of grade 3–4 have a smaller BMI than those with neutrophil deficiencies less than grade 3. **C** Those with a lymphocyte count  $\leq 0.8 \times 10^3/\mu\text{L}$  had a smaller BMI than those with a lymphocyte count  $> 0.8 \times 10^3/\mu\text{L}$ . **D** There was no difference in BMI between those with RBC counts less than or equal to normal and those with RBC counts greater than normal. **E** There was no difference in BMI between those with platelet counts  $\leq 100 \times 10^3/\mu\text{L}$  and those with platelet counts  $> 100 \times 10^3/\mu\text{L}$ . **F** ROC curves of PB WBCs, neutrophils, and lymphocytes according to the BMI values corresponding to the above groupings. **G** There is no difference in dose to the BM between patients with high and low BMI. Results were displayed as mean  $\pm$  SD. ns, not significant; \* $p < 0.05$ ; \*\* $p < 0.01$ , \*\*\* $p < 0.001$ , \*\*\*\* $p < 0.0001$  by unpaired two-tailed Student's  $t$  test. BMI: body mass index.

their lifespan [64]. The current study is the first to discover that irradiation significantly upregulates G6PD and NADPH levels in BM cells and HSPCs of AL mice, indicating activation of PPP. However, DR significantly inhibits the upregulation of G6PD and NADPH. Even high glucose supplementation cannot activate the PPP in HSPCs of DR mice, whereas it further activates the PPP in HSPCs of AL mice. This suggests that DR significantly inhibits the PPP in HSPCs post-irradiation. We also observed that ROS levels in HSPCs of DR mice were significantly higher than those in AL mice post-irradiation. By regulating the PPP, we further revealed its critical role in DNA repair post-irradiation. Based on previous studies, we hypothesize that DR post-irradiation inhibits the activation of PPP, reduces NADPH production, and limits the supply of DNA damage repair substrates. This leads to increased ROS in HSPCs, delayed DNA damage repair, sustained DDR activation, and impaired HSPC function.

Our study also found that DR post-irradiation not only damages hematopoietic cells themselves but also significantly affects the hematopoietic microenvironment. Our research demonstrated that DR post-irradiation can significantly and persistently disrupt the BM microenvironment. DR, administered for both short-term and long-term following irradiation, leads to a significant increase in lipid droplets and a decrease in bone trabeculae in the BM. The increase in lipid droplets and the decrease in bone trabeculae significantly weaken the support for the hematopoietic system [18, 37], thereby exerting a negative regulatory effect on hematopoiesis. This finding is the first to clearly identify the negative regulatory effect of DR on the bone trabeculae and lipid droplets post-irradiation.

Recent studies showed that short-term DR before stress induction, such as chemotherapy and UV radiation, or long-term DR under steady-state conditions, can significantly protect intestinal stem cells, skin, and delay HSC aging [7, 65–67]. The protective effect of pre-stress DR observed in previous research does not contradict the detrimental effect of post-irradiation DR found in the current study. Recent studies show that DR was implemented before the occurrence of stress damage, such as prior to UV irradiation or chemotherapy [65–67]. DR under steady-state conditions (i.e., before the occurrence of damage) can regulate the gut microbiota and initiate a series of protective mechanisms, thereby enhancing resilience against stress when it occurs. Unlike the previous studies, the current study commenced DR only after radiation exposure, without preconditioning the body through DR to establish systemic regulation and protection. Consequently, DR did not exhibit a protective effect on HSCs in this context. A recent publication showed that post-irradiation DR significantly prolongs the quiescent state of hair follicle stem cells and results in higher γH2AX expression in hair follicle cells compared to AL mice [68]. This aligns with our current study's finding that post-irradiation DR significantly inhibits and delays DNA damage repair in hematopoietic cells. This indicates that the effects of pre-stress DR (i.e., DR under steady-state conditions) and post-stress DR are fundamentally different. Pre-stress (steady-state) DR exhibits protective effects through the regulation of the gut microbiome and other potential mechanisms. In contrast, starting DR after irradiation does not allow sufficient time for the gut microbiome and other possible mechanisms to be regulated before the damage occurs, thus highlighting the inhibitory effect

of DR on damage repair. This study complements the previous research by revealing another aspect of DR, showcasing its dual-edged sword effect [17, 69]. We acknowledge that, similar to low BMI, a high BMI may also negatively impact recovery and survival after total body irradiation (TBI), as obese individuals may exhibit altered immune responses and increased systemic inflammation [69]. Investigating these effects in an obese mouse model post-TBI is indeed considered a valuable research direction. In future studies, it will be interesting to use appropriate animal models to explore how both ends of the BMI spectrum—low BMI and high BMI—affect hematopoietic recovery and overall survival after TBI.

The limitations of this study include the fact that, in a clinical setting, radiation therapy for cancer patients aims to minimize damage to normal tissues, including the BM, and patients typically receive myelosuppressive chemotherapy, which was not modeled in our mouse study. The data presented in this study were generated using female C57BL/6J mice. In our mouse model, we used a TBI dose of 4.5 Gy. We confess that TBI is much less often used than targeted region irradiation, which is complicated and difficult in mice in our experimental settings. We also acknowledge that the correlation between doses in animal models and human exposure requires further investigation; thus, caution should be applied when generalizing beyond this scope. The use of mice of the same age and gender in the current study was primarily to reduce variability, as physiological, metabolic, immune, and hematopoietic functions differed significantly between age and gender groups. However, in the real world, patients differ in their age and gender. Therefore, the use of uniform age and gender, as radiation-induced myelosuppression may be influenced by factors such as housing conditions, sex, and genetic background. For example, previous studies indicated that estrogen could promote HSC proliferation [70, 71]. Additionally, anatomical differences and variations in hematopoietic sites between mice and humans, such as the presence of BM in the long bones of mice [72, 73], may affect the translation of these findings to humans.

Furthermore, c-Kit<sup>+</sup> cells represent a mixture of HSPCs at various stages of differentiation and proliferation. Each cell type may respond differently to radiation. Thus, studying the broad category of c-Kit<sup>+</sup> cells as a whole may introduce certain inaccuracies, which we acknowledge as a limitation of our study.

In summary, the current study is the first to discover that DR post-irradiation significantly impairs the function of HSPCs and delays the recovery of BMRMs, osteoblasts and adipocytes in the BM environment. The molecular mechanism was revealed to be the inhibition of DNA damage repair in c-Kit<sup>+</sup> cells through the suppression of PPP activation. This research suggests that the dietary and nutritional status of radiotherapy patients is closely related to radiotherapy-associated hematologic toxicity, providing new insights into addressing radiotherapy-induced BM suppression. It offers potential solutions, particularly for improving refractory hematopoietic disorders associated with radiotherapy. For patients with low BMI, we recommend consultation with a nutritionist to explore methods for enhancing nutritional management and increasing body weight. Potential interventions may include introducing easily digestible and absorbable nutritional supplements and foods, utilizing intravenous nutritional support, and incorporating probiotics to promote digestion and absorption. These approaches could potentially ameliorate hematopoietic toxicity of low BMI patients induced by radiotherapy of low BMI patients to radiotherapy.

## DATA AVAILABILITY

All data needed to evaluate the conclusions in the paper are present in the paper and/or the Supplementary Materials.

## REFERENCES

- Wang K, Tepper JE. Radiation therapy-associated toxicity: Etiology, management, and prevention. *CA Cancer J Clin*. 2021;71:437–54.
- Shao L, Luo Y, Zhou D. Hematopoietic stem cell injury induced by ionizing radiation. *Antioxidants Redox Signal*. 2014;20:1447–62.
- Ng SP, Bahig H, Jethanandani A, Pollard C, Berends J, Sturgis EM, et al. Lymphopenia during radiotherapy in patients with oropharyngeal cancer. *Radiother Oncol*: J Eur Soc Ther Radiol Oncol. 2020;145:95–100.
- Iorio GC, Spieler BO, Ricardi U, Dal Pra A. The impact of pelvic nodal radiotherapy on hematologic toxicity: a systematic review with focus on leukopenia, lymphopenia and future perspectives in prostate cancer treatment. *Crit Rev Oncol Hematol*. 2021;168:103497.
- Morrison SJ, Scadden DT. The bone marrow niche for haematopoietic stem cells. *Nature*. 2014;505:327–34.
- Tang D, Tao S, Chen Z, Kolesnik IO, Calmes PG, Hoerr V, et al. Dietary restriction improves repopulation but impairs lymphoid differentiation capacity of hematopoietic stem cells in early aging. *J Exp Med*. 2016;213:535–53.
- Tao S, Wang Y, Wu J, Zeng T, Cui H, Tao Z, et al. Long-term mid-onset dietary restriction rejuvenates hematopoietic stem cells and improves regeneration capacity of total bone marrow from aged mice. *Aging Cell*. 2020;19:e13241.
- Mattison JA, Colman RJ, Beasley TM, Allison DB, Kemnitz JW, Roth GS, et al. Caloric restriction improves health and survival of rhesus monkeys. *Nat Commun*. 2017;8:14063.
- Khalafi M, Habibi Maleki A, Symonds ME, Rosenkranz SK, Rohani H, Ehsanifar M. The effects of intermittent fasting on body composition and cardiometabolic health in adults with prediabetes or type 2 diabetes: a systematic review and meta-analysis. *Diabetes Obes Metab*. 2024;26:3830–41.
- McCay CM, Crowell MF, Maynard LA. The effect of retarded growth upon the length of life span and upon the ultimate body size. 1935. *Nutrition*. 1989;5:155–71. Discussion 72.
- Islam MM, Sultana N, Liu C, Mao A, Katsume T, Wang B. Impact of dietary ingredients on radioprotection and radiosensitization: a comprehensive review. *Ann Med*. 2024;56:2396558.
- Icard P, Ollivier L, Forgez P, Otz J, Alifano M, Fournel L, et al. Perspective: do fasting, caloric restriction, and diets increase sensitivity to radiotherapy? A literature review. *Adv Nutr*. 2020;11:1089–101.
- Muhammad N, Ruiz F, Stanley J, Rashmi R, Cho K, Jayachandran K, et al. Mono-unsaturated and diunsaturated fatty acids sensitize cervical cancer to radiation therapy. *Cancer Res*. 2022;82:4515–27.
- Pepoyan AZ, Manvelyan AM, Balayan MH, McCabe G, Tsaturyan VV, Melnikov VG, et al. The effectiveness of potential probiotics *Lactobacillus rhamnosus* Vahe and *Lactobacillus delbrueckii* IAHAHI in irradiated rats depends on the nutritional stage of the host. *Probiot Antimicrob Proteins*. 2020;12:1439–50.
- Lu L, Li F, Gao Y, Kang S, Li J, Guo J. Microbiome in radiotherapy: an emerging approach to enhance treatment efficacy and reduce tissue injury. *Mol Med*. 2024;30:105.
- Liu J, Liu C, Yue J. Radiotherapy and the gut microbiome: facts and fiction. *Radiat Oncol*. 2021;16:9.
- Ellis SL, Grassinger J, Jones A, Borg J, Camenisch T, Haylock D, et al. The relationship between bone, hemopoietic stem cells, and vasculature. *Blood*. 2011;118:1516–24.
- Hayashi Y, Kawabata KC, Tanaka Y, Uehara Y, Kiryu S, Ota Y, et al. Impaired osteoblastic differentiation of MSCs suppresses normal hematopoiesis in MDS. *Blood*. 2020;136:17–8.
- Green DE, Rubin CT. Consequences of irradiation on bone and marrow phenotypes, and its relation to disruption of hematopoietic precursors. *Bone*. 2014;63:87–94.
- Sawai CM, Babovic S, Upadhyaya S, Knapp D, Lavin Y, Lau CM, et al. Hematopoietic stem cells are the major source of multilineage hematopoiesis in adult animals. *Immunity*. 2016;45:597–609.
- Pucella JN, Upadhyaya S, Reizis B. The source and dynamics of adult hematopoiesis: insights from lineage tracing. *Annu Rev Cell Dev Biol*. 2020;36:529–50.
- Mendelson A, Frenette PS. Hematopoietic stem cell niche maintenance during homeostasis and regeneration. *Nat Med*. 2014;20:833–46.
- Hu L, Yin X, Zhang Y, Pang A, Xie X, Yang S, et al. Radiation-induced bystander effects impair transplanted human hematopoietic stem cells via oxidative DNA damage. *Blood*. 2021;137:3339–50.
- Rodrigues-Moreira S, Moreno SG, Ghinatti G, Lewandowski D, Hoffschir F, Ferri F, et al. Low-dose irradiation promotes persistent oxidative stress and decreases self-renewal in hematopoietic stem cells. *Cell Rep*. 2017;20:3199–211.
- Cosentino C, Grieco D, Costanzo V. ATM activates the pentose phosphate pathway promoting anti-oxidant defence and DNA repair. *EMBO J*. 2011;30:546–55.
- Jones NP, Schulze A. Targeting cancer metabolism—aiming at a tumour's sweet-spot. *Drug Discov Today*. 2012;17:232–41.

27. Mohrin M, Bourke E, Alexander D, Warr MR, Barry-Holton K, Le Beau MM, et al. Hematopoietic stem cell quiescence promotes error-prone DNA repair and mutagenesis. *Cell Stem Cell*. 2010;7:174–85.

28. Cui H, Tang D, Garside GB, Zeng T, Wang Y, Tao Z, et al. Wnt signaling mediates the aging-induced differentiation impairment of intestinal stem cells. *Stem Cell Rev Rep*. 2019;15:448–55.

29. Donaldson SS. Nutritional consequences of radiotherapy. *Cancer Res*. 1977;37:2407–13.

30. Capra S, Ferguson M, Ried K. Cancer: impact of nutrition intervention outcome–nutrition issues for patients. *Nutrition*. 2001;17:769–72.

31. Doyle SL, Donohoe CL, Lysaght J, Reynolds JV. Visceral obesity, metabolic syndrome, insulin resistance and cancer. *Proc Nutr Soc*. 2012;71:181–9.

32. Kenchaiah S, Evans JC, Levy D, Wilson PW, Benjamin EJ, Larson MG, et al. Obesity and the risk of heart failure. *New Engl J Med*. 2002;347:305–13.

33. Oreopoulos A, Padwal R, Kalantar-Zadeh K, Fonarow GC, Norris CM, McAlister FA. Body mass index and mortality in heart failure: a meta-analysis. *Am Heart J*. 2008;156:13–22.

34. Bhaskaran K, Douglas I, Forbes H, dos-Santos-Silva I, Leon DA, Smeeth L. Body-mass index and risk of 22 specific cancers: a population-based cohort study of 5.24 million UK adults. *Lancet*. 2014;384:755–65.

35. Kalantar-Zadeh K, Block G, Horwitz T, Fonarow GC. Reverse epidemiology of conventional cardiovascular risk factors in patients with chronic heart failure. *J Am Coll Cardiol*. 2004;43:1439–44.

36. Chalot M, Barroca V, Devanand S, Hoffschir F, Romeo PH, Moreno SG. deleterious effect of bone marrow-resident macrophages on hematopoietic stem cells in response to total body irradiation. *Blood Adv*. 2022;6:1766–79.

37. Naveiras O, Nardi V, Wenzel PL, Hauschka PV, Fahey F, Daley GQ. Bone-marrow adipocytes as negative regulators of the haematopoietic microenvironment. *Nature*. 2009;460:259–63.

38. Ciccia A, Elledge SJ. The DNA damage response: making it safe to play with knives. *Mol Cell*. 2010;40:179–204.

39. Ghosh S, Ghosh A. Activation of DNA damage response signaling in mammalian cells by ionizing radiation. *Free Radic Res*. 2021;55:581–94.

40. Bourguignon MH, Gisone PA, Perez MR, Michelin S, Dubner D, Giorgio MD, et al. Genetic and epigenetic features in radiation sensitivity Part I: cell signalling in radiation response. *Eur J Nucl Med Mol Imaging*. 2005;32:229–46.

41. Schirolí G, Conti A, Ferrari S, Della Volpe L, Jacob A, Albano L, et al. Precise gene editing preserves hematopoietic stem cell function following transient p53-mediated DNA damage response. *Cell Stem Cell*. 2019;24:551–65.e8.

42. Nijnik A, Woodbine L, Marchetti C, Dawson S, Lambe T, Liu C, et al. DNA repair is limiting for haematopoietic stem cells during ageing. *Nature*. 2007;447:686–90.

43. de Feraudy S, Revet I, Bezrookove V, Feeney L, Cleaver JE. A minority of foci or pan-nuclear apoptotic staining of gammaH2AX in the S phase after UV damage contain DNA double-strand breaks. *Proceedings Natl Acad Sci USA*. 2010;107:6870–5.

44. Tao S, Wang Y, Yu C, Qiu R, Jiang Y, Jia J, et al. Gut microbiota mediates the inhibition of lymphopoiesis in dietary-restricted mice by suppressing glycolysis. *Gut Microbes*. 2022;14:2117509.

45. Ju HQ, Lin JF, Tian T, Xie D, Xu RH. NADPH homeostasis in cancer: functions, mechanisms and therapeutic implications. *Signal Transduct Target Ther*. 2020;5:231.

46. TeSlaa T, Ralser M, Fan J, Rabinowitz JD. The pentose phosphate pathway in health and disease. *Nat Metab*. 2023;5:1275–89.

47. Jiang P, Du W, Wu M. Regulation of the pentose phosphate pathway in cancer. *Protein Cell*. 2014;5:592–602.

48. Ahmed SM, Luo L, Namanji A, Wang XJ, Tang X. Nrf2 signaling pathway: pivotal roles in inflammation. *Biochim Biophys Acta Mol Basis Dis*. 2017;1863:585–97.

49. DeNicola GM, Karreth FA, Humpton TJ, Gopinathan A, Wei C, Frese K, et al. Oncogene-induced Nrf2 transcription promotes ROS detoxification and tumorigenesis. *Nature*. 2011;475:106–9.

50. Ma Q. Role of nrf2 in oxidative stress and toxicity. *Annu Rev Pharm Toxicol*. 2013;53:401–26.

51. Sharma PK, Bhardwaj R, Dwarakanath BS, Varshney R. Metabolic oxidative stress induced by a combination of 2-DG and 6-AN enhances radiation damage selectively in malignant cells via non-coordinated expression of antioxidant enzymes. *Cancer Lett*. 2010;295:154–66.

52. Ghergurovich JM, García-Cañavera JC, Wang J, Schmidt E, Zhang Z, TeSlaa T, et al. A small molecule G6PD inhibitor reveals immune dependence on pentose phosphate pathway. *Nature Chem Biol*. 2020;16:731–9.

53. Hwang S, Mruk K, Rahighi S, Raub AG, Chen C-H, Dorn LE, et al. Correcting glucose-6-phosphate dehydrogenase deficiency with a small-molecule activator. *Nat Commun*. 2018;9:4045.

54. Ryan K, Tekwani BL. Current investigations on clinical pharmacology and therapeutics of glucose-6-phosphate dehydrogenase deficiency. *Pharmacol Ther*. 2021;222:107788.

55. Ikushima H, Osaki K, Furutani S, Yamashita K, Kishida Y, Kudoh T, et al. Pelvic bone complications following radiation therapy of gynecologic malignancies: clinical evaluation of radiation-induced pelvic insufficiency fractures. *Gynecol Oncol*. 2006;103:1100–4.

56. Shahid S. Review of hematological indices of cancer patients receiving combined chemotherapy & radiotherapy or receiving radiotherapy alone. *Crit Rev Oncol/Hematol*. 2016;105:145–55.

57. Wang Y, Schulte BA, LaRue AC, Ogawa M, Zhou D. Total body irradiation selectively induces murine hematopoietic stem cell senescence. *Blood*. 2006;107:358–66.

58. Lane AN, Fan TW. Regulation of mammalian nucleotide metabolism and biosynthesis. *Nucleic Acids Res*. 2015;43:2466–85.

59. Tree AC, Khoo VS, Eeles RA, Ahmed M, Dearnaley DP, Hawkins MA, et al. Stereotactic body radiotherapy for oligometastases. *Lancet Oncol*. 2013;14:e28–37.

60. Zhou P, Zhang Y, Luo S, Zhang S. Pelvic bone marrow sparing radiotherapy for cervical cancer: a systematic review and meta-analysis. *Radiother Oncol*. 2021;165:103–18.

61. Demeyer A, Benhelli-Mokrani H, Chénais B, Weigel P, Fleury F. Inhibiting homologous recombination by targeting RAD51 protein. *Biochim Biophys Acta Rev Cancer*. 2021;1876:188597.

62. Wang Y, Liu L, Pazhanisamy SK, Li H, Meng A, Zhou D. Total body irradiation causes residual bone marrow injury by induction of persistent oxidative stress in murine hematopoietic stem cells. *Free Radic Biol Med*. 2010;48:348–56.

63. Patra KC, Hay N. The pentose phosphate pathway and cancer. *Trends Biochem Sci*. 2014;39:347–54.

64. Nóbrega-Pereira S, Fernandez-Marcos PJ, Brioche T, Gomez-Cabrera MC, Salvador-Pascual A, Flores JM, et al. G6PD protects from oxidative damage and improves healthspan in mice. *Nat Commun*. 2016;7:10894.

65. Tang D, Zeng T, Wang Y, Cui H, Wu J, Zou B, et al. Dietary restriction increases protective gut bacteria to rescue lethal methotrexate-induced intestinal toxicity. *Gut Microbes* 2020;12:1714401.

66. Tang D, Wu J, Wang Y, Cui H, Tao Z, Lei L, et al. Dietary restriction attenuates inflammation and protects mouse skin from high-dose ultraviolet B irradiation. *Rejuvenation Res*. 2022;25:149–57.

67. Tang D, Qiu R, Qiu X, Sun M, Su M, Tao Z, et al. Dietary restriction rescues 5-fluorouracil-induced lethal intestinal toxicity in old mice by blocking translocation of opportunistic pathogens. *Gut Microbes*. 2024;16:2355693.

68. Qiu R, Qiu X, Su M, Sun M, Wang Y, Wu J, et al. Dietary restriction delays but cannot heal irradiation-induced hair graying by preserving hair follicle stem cells in quiescence. *Rejuvenation Res*. 2023;26:242–52.

69. Zhang Y, Yang X, Zhuang Z, Wei M, Meng W, Deng X, et al. The effect of BMI on long-term outcome in patients with rectal cancer and establishment of a nomogram prediction model. *BMC Gastroenterol*. 2023;23:5.

70. Oguro H, McDonald JG, Zhao Z, Umetani M, Shaul PW, Morrison SJ. 27-Hydroxycholesterol induces hematopoietic stem cell mobilization and extramedullary hematopoiesis during pregnancy. *J Clin Investig*. 2017;127:3392–401.

71. Kiang JG, Cannon G, Olson MG, Smith JT, Anderson MN, Zhai M, et al. Female mice are more resistant to the mixed-field (67% neutron + 33% gamma) radiation-induced injury in bone marrow and small intestine than male mice due to sustained increases in G-CSF and the Bcl-2/bax ratio and lower miR-34a and MAPK activation. *Radiat Res*. 2022;198:120–33.

72. Kent DG. Different roles for different bones—location matters for blood production. *Hemisphere*. 2024;8:e127.

73. Pinho S, Frenette PS. Haematopoietic stem cell activity and interactions with the niche. *Nat Rev Mol Cell Biol*. 2019;20:303–20.

## ACKNOWLEDGEMENTS

This work was supported by the National Natural Science Fund of China (NSFC-82360287 and NSFC-82160029) and the Jiangxi Provincial Nature Science Foundation (20232ACB206014).

## AUTHOR CONTRIBUTIONS

S.T. and M.S. performed and analyzed the majority of the experiments. C.Y. participated in most experiments. X.Q., R.Q. and Y.W. assisted with mouse experiments and manuscript preparation. B.Z. calculated irradiation doses for patients. L.L., D.T., L.Z. and H.W. contributed to patient data collection and analysis and provided suggestions. D.T. and S.T. conceived and designed the study. The manuscript was written by S.T., M.S. and D.T. and critically revised by all authors.

**COMPETING INTERESTS**

The authors declare no competing interests.

**ADDITIONAL INFORMATION**

**Supplementary information** The online version contains supplementary material available at <https://doi.org/10.1038/s41419-025-08249-w>.

**Correspondence** and requests for materials should be addressed to Duozhuang Tang.

**Reprints and permission information** is available at <http://www.nature.com/reprints>

**Publisher's note** Springer Nature remains neutral with regard to jurisdictional claims in published maps and institutional affiliations.



**Open Access** This article is licensed under a Creative Commons Attribution 4.0 International License, which permits use, sharing, adaptation, distribution and reproduction in any medium or format, as long as you give appropriate credit to the original author(s) and the source, provide a link to the Creative Commons licence, and indicate if changes were made. The images or other third party material in this article are included in the article's Creative Commons licence, unless indicated otherwise in a credit line to the material. If material is not included in the article's Creative Commons licence and your intended use is not permitted by statutory regulation or exceeds the permitted use, you will need to obtain permission directly from the copyright holder. To view a copy of this licence, visit <http://creativecommons.org/licenses/by/4.0/>.

© The Author(s) 2025